Article

Remote activation of place codes by gaze in a highly visual animal

https://doi.org/10.1038/s41586-025-09101-z

Received: 27 September 2024

Accepted: 6 May 2025

Published online: 11 June 2025

Check for updates

Hannah L. Payne[1]✉ & Dmitriy Aronov[1,2]✉

Vision enables many animals to perform spatial reasoning from remote locations[1]. By viewing distant landmarks, animals recall spatial memories and plan future trajectories. Although these spatial functions depend on hippocampal place cells[2,3], the relationship between place cells and active visual behaviour is unknown. Here we studied a highly visual animal, the chickadee, in a behaviour that required alternating between remote visual search and spatial navigation. We leveraged the head-directed nature of avian vision to track gaze in freely moving animals. We discovered a profound link between place coding and gaze. Place cells activated not only when the chickadee was in a specific location, but also when it simply gazed at that location from a distance. Gaze coding was precisely timed by fast ballistic head movements called 'head saccades'[4,5]. On each saccadic cycle, the hippocampus switched between encoding a prediction of what the bird was about to see and a reaction to what it actually saw. The temporal structure of these responses was coordinated by subclasses of interneurons that fired at different phases of the saccade. We suggest that place and gaze coding are components of a unified process by which the hippocampus represents the location that is relevant to the animal in each moment. This process allows the hippocampus to implement both local and remote spatial functions.

Consider a classic example of spatial memory: an animal remembering a nut hidden at the base of a tree. Theories of hippocampal function posit that such a memory depends on place cells—in this case, the set of neurons active at the base of the tree[2,3]. Therein lies a problem: to efficiently find the tree and retrieve the nut, the animal must first recall the memory from a remote location where a completely different set of place cells might be active. How are place cells compatible with such a remote function of the hippocampus? In visual animals, remote recall is often driven by gaze[1]. By simply looking at a place from a distance, animals can recall associated information without physically revisiting that location. Yet, it is unknown how the brain coordinates remote vision with the activity of place cells.

This problem is unsolved largely because eye tracking in freely behaving animals is extremely challenging. In addition to this technical issue, many laboratory models, including rodents, lack foveal vision[4] and rarely orient their eyes precisely at visual targets. It is often impossible to know exactly what these animals are looking at, even when eye tracking is feasible[6–9]. In primates with foveal vision, some hippocampal activity is correlated with gaze location[10–15] and other visual information[16–18]. However, these animals are usually recorded stationary or in conditions where it is hard to disambiguate gaze coding from place coding.

To address these challenges, we leveraged a unique feature of avian biology. Birds, like primates, have foveal vision and actively control their gaze to fixate visual targets[4,5,19]. However, instead of eye movements, many bird species rely primarily on head movements to shift gaze from one target to another. These head movements are much more feasible to track in small, freely moving animals. We chose to use the black-capped chickadee, a member of a food-caching bird family that has abundant place cells in the hippocampus[20,21]. Chickadees provide a unique opportunity to study spatial coding and gaze simultaneously during unconstrained behaviour.

Head-directed gaze strategies in chickadees

All birds use their heads to direct gaze, but the nature of head movements and the extent of additional eye movements are highly variable across species[4,22]. Therefore, we started by characterizing these behaviours in chickadees. For head tracking, we adapted a multi-camera system[23] that triangulated infrared-reflective markers on the bird's head (Fig. 1a). As in other species[4,5], these measurements revealed a saccadic-like behaviour (Fig. 1b). Chickadees produced fast ballistic changes in head angle ('head saccades') interleaved with periods of stable head angle ('gaze fixations'). Head saccades were 76 ± 21 ms in duration, occurred at instantaneous rates of 3.8 ± 1.4 Hz and were in several additional ways remarkably similar to eye saccades in primates[1] (mean ± s.d.; $n = 3.3 \times 10^5$ saccades in eight birds; Fig. 1c and Extended Data Fig. 1a–c).

We then performed a calibration experiment in which we tracked eye movements in addition to head movements. For this purpose, we engineered a dual-camera video-oculography system that estimates the pupillary axis using corneal reflections from two infrared light sources (Fig. 1a and Extended Data Fig. 2). These measurements were possible only when we encouraged the chickadees to perch directly in front of the cameras. We found very little movement of the eyes relative to the head: 5.4 ± 0.4° median absolute deviation, nearly an

[1]Zuckerman Mind Brain Behavior Institute, Columbia University, New York, NY, USA. [2]Howard Hughes Medical Institute at Columbia University, New York, NY, USA. ✉e-mail: hannah.payne@columbia.edu; da2006@columbia.edu

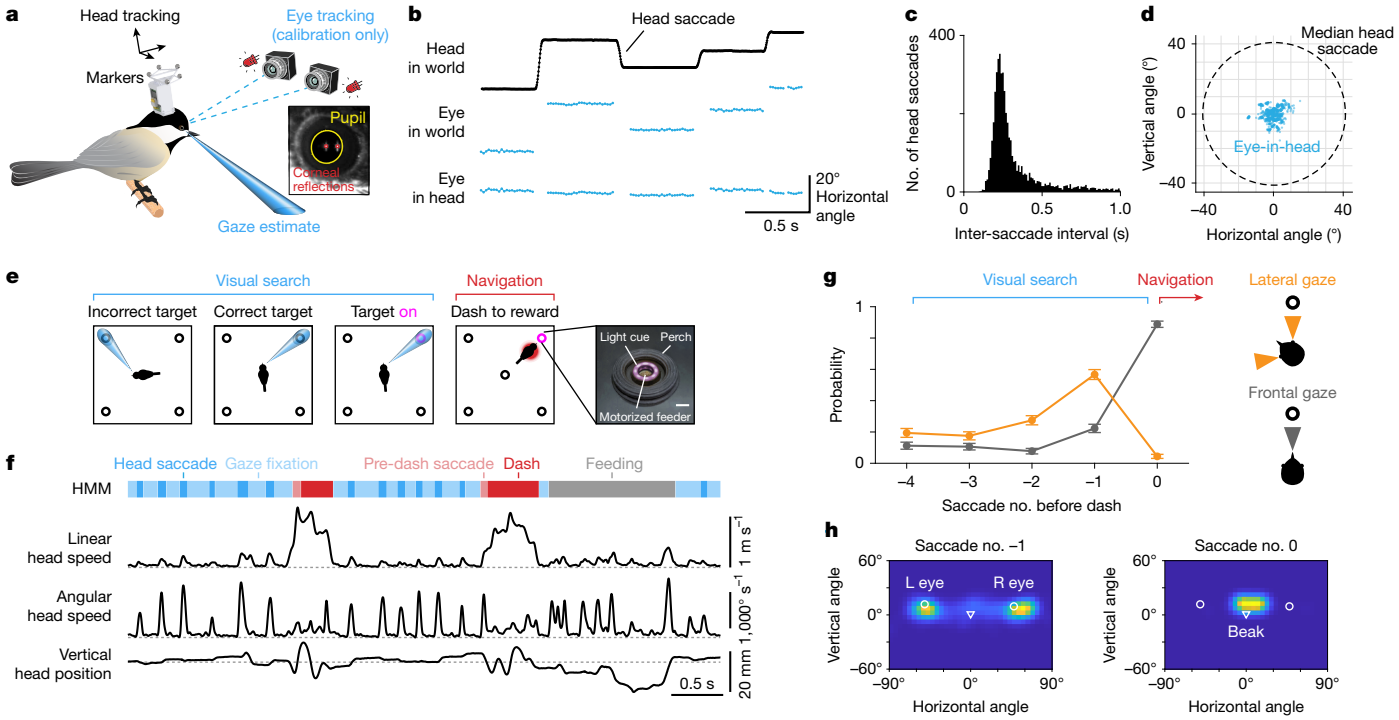

Fig. 1 | Head-directed gaze strategies in chickadees. a, Head position was tracked using four infrared cameras (not shown) and reflective markers on the head. In a calibration experiment, eye position was measured using two extra cameras that tracked the pupil and corneal reflections from two light sources. **b**, Head angle showed prolonged fixations interrupted by fast ballistic movements ('head saccades'). For simplicity, only the horizontal angle is plotted. The eye could not be accurately tracked during head saccades; therefore, these points are omitted. When head position was subtracted from eye position, the residual eye position relative to the head showed very little movement. **c**, Distribution of intervals between head saccades from a single session. **d**, Distribution of eye positions from an example calibration experiment. Eye movements relative to the head were much smaller than the head saccades. **e**, Schematic of the discrete visual search task, which includes a visual search period and a separate navigational period. Gaze at the correct target activates a light cue. The chickadee then navigates to that target to obtain a reward. **f**, Different behaviours involve distinct movements of the head and could be segmented from the head tracking data using a HMM. **g**, Time course of the bird's use of two different gaze strategies (lateral and frontal gaze). Saccade 0 is defined as the one immediately preceding a dash ('pre-dash saccade' in **f**). Error bars represent the mean ± standard error of the binomial proportion for one example session (n = 250 dashes). **h**, Distribution of head orientations relative to the target, averaged across all instances of saccade 0 and saccade −1 for the same bird as in **g**. Symbols mark the orientation of the two pupil centres and the tip of the beak. Saccade 0 was usually frontal (using both eyes). Before that, the saccades tended to be lateral (using one eye at a time). Scale bar, 1 cm (**e** (rightmost)).

order of magnitude smaller than the movement of the head itself (n = 8 birds; Fig. 1b,d and Extended Data Fig. 2f). We conclude that chickadees almost exclusively rely on head saccades to direct their gaze during free motion. Therefore, head tracking is sufficient to determine where a bird is looking, provided that gaze targets in a behavioural task are separated by more than approximately 10°. Unlike eye tracking, which requires the head to be nearly stationary relative to the camera, head tracking is feasible in chickadees freely navigating across a behavioural arena.

To study place and gaze coding, we trained chickadees on a discrete visual search task (Fig. 1e and Supplementary Video 1). The bird visited five visually identical sites: one at the centre and four near the corners of a 61-cm arena. Each site consisted of a perch, a light cue and a motorized feeder. In each trial, one of the four corner sites was randomly chosen as the rewarded location. The chickadee started the trial by perching at the central site. The rewarded site was indicated by a light. Once the light turned on, the bird approached the indicated site to retrieve a piece of sunflower seed and then returned to the centre to initiate a new trial. Chickadees typically approached sites with fast, direct movements that we call 'dashes'. Although the arena was two-dimensional, these dashes typically covered only the X-shaped region that connected the centre with the corner sites. We used a hidden Markov model (HMM) to segment dashes, gaze fixations, saccades and feeding periods in the head tracking data (Fig. 1f). Chickadees performed 163–304 trials (25th–75th percentile; n = 58 sessions across both tasks described below), with each site rewarded in roughly one-quarter of the trials in any given session.

We first ran a simple version of the task to characterize the chickadees' visual search behaviour. In this version, the light cue of the rewarded site turned on after a random delay (up to 5 s) from the start of the trial. We found that chickadees used two distinct gaze strategies in our task (Fig. 1g,h and Extended Data Fig. 1d). During the delay period, they shifted their gaze between different sites by using one eye at a time ('lateral gaze'). In other words, chickadees oriented their heads to align either the left or the right pupil with one of the sites. Because the light cue was intentionally dim, chickadees probably used this behaviour to search for the correct site using the foveal region of the retina[19]. After locating the light, birds instead oriented their beaks towards the target ('frontal gaze'), viewing the rewarded site with the non-foveal region of both eyes. They usually followed this frontal gaze with a dash. Other bird species use similar strategies, relying on lateral gaze to investigate objects and frontal gaze during directed movements[24–26].

Considering these results, we modified the task to create a closed-loop version. Instead of enforcing a delay period, we activated the light cue in response to the bird gazing at the correct site. Because chickadees had no a priori knowledge of which site was rewarded, they often gazed at several incorrect sites before choosing the correct one. The closed-loop structure allowed us to precisely control the timing of the visual stimulus relative to the saccade. This also ensured that the cue was not detectable by peripheral vision during off-target saccades; this feature will become important later. In this closed-loop task, we recorded activity in the anterior hippocampus (Extended Data Fig. 3) using silicon probes.

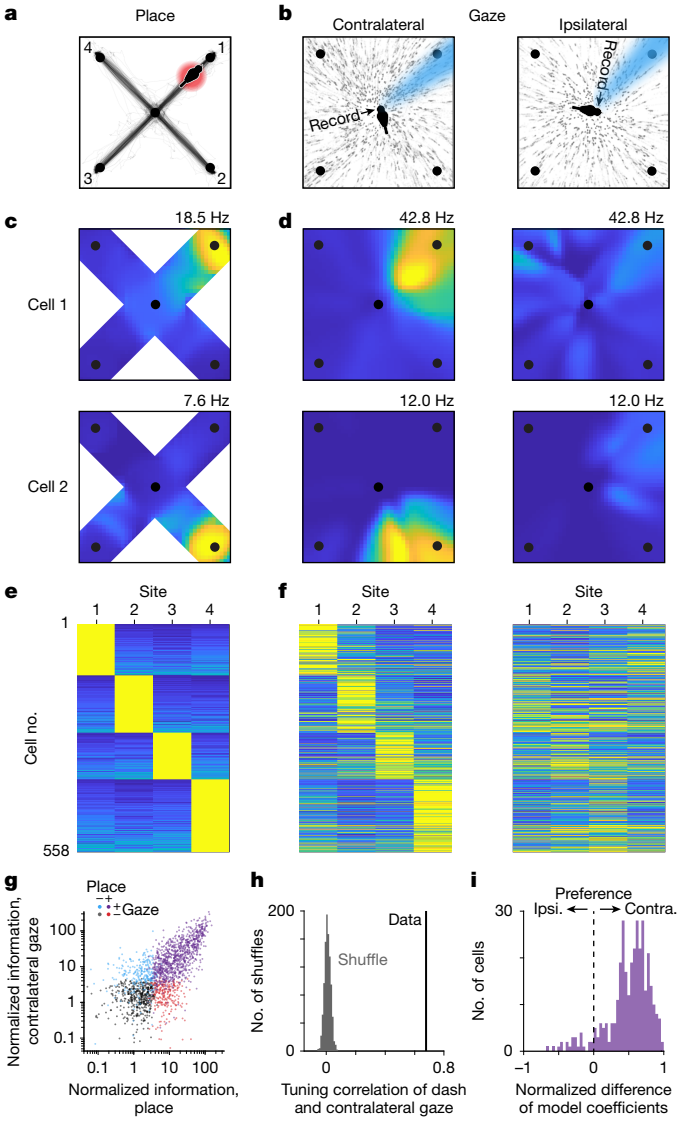

Fig. 2 | Place cells are activated by remote gaze. a, Place representations were measured during times when the bird was dashing towards an outer target site. Black trace: trajectory of the bird during such time periods in a single example session. This trajectory was mostly confined to the X-shaped portion of the arena that connected the target sites (1–4) to the centre site. **b**, Gaze representation was measured during times when the bird was saccading from the centre of the arena. Black dots: projected gaze in the same example session, plotted separately for the eyes contralateral and ipsilateral to the hippocampal recording. **c**, Mean firing rate as a function of the bird's location for two example place cells. Only locations on the X-shaped part of the arena are shown, because the chickadee almost never visited other locations. The colour scale ranges from 0 (blue) to the indicated maximum (yellow). **d**, Mean firing rate as a function of gaze location for the same two cells. **e**, Peak firing rate during dashes to each of the four target sites. Excitatory place cells with strong place selectivity for one of the sites (greater than 0.5 selectivity index) are shown. Cells are sorted first by the location of their strongest response, and then by the magnitude of their second strongest response. Each row is normalized separately from 0 (blue) to the maximum (yellow). **f**, Coefficients of a model that fits gaze responses as a combination of tuning to contralateral and ipsilateral gaze. Cells and sorting are the same as those described in **e**. Rows are normalized to the maximum across both matrices in **f**. Note that cells are not excluded from this plot on the basis of their gaze responses; the relationship between place and gaze tuning is shown across the entire population of place cells. **g**, Strength of place and gaze tuning across all excitatory cells. Cells are coloured on the basis of a statistical threshold for place and/or gaze tuning; these colours are not meant to represent separable classes of neurons. 'Normalized information' is mutual information between spikes and the behavioural variable (place or contralateral gaze, discretized into four target sites), divided by the mean for shuffled data. The two types of tuning are strongly correlated. **h**, Correlation of tuning curves for place and contralateral gaze ($r = 0.68$; $n = 558$ cells). Tuning curves were measured across the four target sites for all place cells, as shown in **e** and **f**. The shuffled distribution was obtained by scrambling cell identities. **i**, Comparison of contralateral (contra.) and ipsilateral (ipsi.) gaze responses using model coefficients in **f** for each cell's preferred dash target. Included cells are those in **h** with greater than 0.5 selectivity for both place and gaze with at least one of the eyes ($n = 289$ cells). The normalized difference was calculated as $(c - i)/(c + i)$, where c and i are the contralateral and ipsilateral coefficients, respectively. Gaze responses are almost entirely explained by contralateral tuning.

Place cells are activated by remote gaze

We measured place tuning and gaze tuning in the firing of hippocampal neurons. To match published studies[20,21,27], we analysed place tuning only during periods when the chickadee was locomoting—that is, during dashes between sites (Fig. 2a). By contrast, we analysed gaze tuning during stationary visual search periods when the bird was saccading and fixating from the central perch (Fig. 2b). We started by examining the activity as a function of gaze from the eye contralateral to our hippocampal recording ('contralateral gaze'). To quantify place and gaze tuning, we measured firing rates during dashes and gazes, respectively, at each of the four target sites. We then computed mutual information between firing rate and site identity. As in other behavioural tasks, many hippocampal neurons in chickadees were place-tuned: of the 1,929 putative excitatory cells in seven birds, 62% were classified as place cells ($P < 0.01$; mutual information compared with shuffled data). We found that a similarly large fraction of cells were gaze-tuned: 57% of the same 1,929 neurons ($P < 0.01$). Many of these cells had strong gaze fields that were tightly localized in the environment, qualitatively similar to conventional place fields (Fig. 2c,d).

There are other known situations in which the hippocampus encodes more than one experimental variable[3,18,20,28,29]. In these cases, different types of selectivity are usually mixed randomly in the recorded population. However, this was not the case for place and gaze tuning. The amounts of information encoded about place and gaze were strongly correlated across cells (Fig. 2e–g). In fact, 75% of all place cells were also significantly tuned to gaze, compared with 57% expected from random mixing.

Not only did the same neurons encode place and gaze, but these two representations also had a striking overlap in space (Fig. 2c,d). To quantify this overlap, we selected place cells that had a strong preference for dashes towards a single site. Tuning curves for place and gaze were strongly correlated in these cells (Fig. 2e,f,h). In those cells that also had a strong preference for a single gaze target, the preferred place was the same as the preferred gaze in 95% of cases, compared with approximately 25% expected by chance. These analyses show that place and gaze tuning are not represented independently in the hippocampus. Rather, remote gaze activates place representations. In other words, a place cell is active not only when a bird is physically in a certain location but also when the bird simply looks at that location from a distance.

In many behaviours, the hippocampus can represent the future location of the animal[30,31]. In our task, birds often looked at sites before visiting them. Therefore, a conceivable explanation of our results is that the hippocampus actually represents future location, which happens to correlate with gaze. To determine whether gaze responses were specifically related to visual behaviour, we relied on a unique feature of avian anatomy. As in mammals, the avian hippocampus receives input from multiple visual pathways[32–34]. However, in most birds, the optic tract fully crosses the contralateral hemisphere at the optic chiasm[35]. There is also very limited cross-hemispheric communication in the visual system due to the lack of a corpus callosum. As a result, visual functions are highly lateralized[36,37]. If gaze signals are actually driven

by future location, we should observe them bilaterally. However, if they are specific to gaze, we might expect them to be lateralized in the hippocampus.

We observed place and gaze tuning in both hemispheres. However, gaze tuning was evident only when we analysed the eye contralateral to the recorded hippocampus (Fig. 2d). Neurons responded only when the contralateral eye, but not the ipsilateral eye, looked at the preferred target. To illustrate this result across the population, we implemented a model that fit neural activity as a combination of tuning to ipsilateral and contralateral gaze. Such a model was necessary because the chickadees sometimes gazed simultaneously at two sites with different eyes. In this model, activity was almost entirely explained by contralateral gaze (Fig. 2f,i). This result was true regardless of whether birds were allowed to use either eye or only the contralateral eye to trigger the reward (Extended Data Fig. 4). We conclude that gaze tuning is specific to where the bird is looking.

Are responses during dashes truly tuned to the bird's location? Because place and gaze tuning overlap, an alternative is that apparent place coding during dashes can be explained by visual responses to the target sites. We considered this to be unlikely. First, all four targets were visually identical. Therefore, spatially selective gaze responses had to depend on the spatial arrangement of distant landmarks, not only the local features of the target sites. Second, targets looked very different to birds during gazes and dashes yet produced similar responses. During gazes, targets were viewed by the foveal part of the retina and appeared small because of their large distance from the bird. During dashes, they were viewed by the non-foveal part of the retina and appeared several times larger. To further rule out visual responses, we analysed periods of time when the chickadee arrived at the target site but was no longer looking at it. Cells retained their place selectivity during these times, regardless of which way the bird was facing and whether the light cue turned on or off (Extended Data Fig. 5a–f). We also found that very few cells responded to the light cue without regard for its location (Extended Data Fig. 5g,h). Finally, we identified many cells with place fields along the paths to the targets rather than directly at the targets (Extended Data Fig. 6). We conclude that chickadee hippocampal activity is truly spatial and cannot be explained by visual responses to target sites or the reward indicator light.

Another consideration is that in the 'X-shaped' task presented so far, chickadees always performed the visual search from the same central location of the arena. Could hippocampal activity encode the direction of gaze, rather than the location of the gaze target? We could not test this possibility in the X-shaped task because chickadees rarely gazed at any site when they were not perched at the centre. Therefore, we trained three birds on a separate 'all-to-all' task, in which they dashed directly between five outer target sites without returning to a central perch (Extended Data Fig. 7). We found that gaze responses depended on both the site where the chickadee was located (the 'source') and the site at which it was looking (the 'target'). Responses for the same target from different sources were more similar than responses for different targets from the same source. We conclude that gaze responses predominantly encoded the location of the visual target, although they were also partially affected by the location of the bird. These responses cannot be explained by the direction of gaze alone.

Gaze responses encode an internal prediction

An overarching question in our study is whether the hippocampus can recall internal information about the visual world. For this purpose, it is not sufficient to simply react to visual stimuli; rather, neural responses should contain additional, internally driven information about the gaze targets. To test this idea, we first asked whether the timing of gaze activity was consistent with a purely sensory response. We aligned neural activity to the time of peak angular head velocity during each saccade separately for each target site. We compared these responses to the timing of activity during dashes. Unexpectedly, we found that the saccade-aligned activity, but not the dash-aligned activity, was biphasic (Fig. 3a–d). Neurons produced the first peak in firing ('early response') during the saccade itself at 17 ± 14 ms and then the second peak ('late response') at 187 ± 4 ms (n = 278 place-selective and gaze-selective cells; mean ± bootstrapped standard error; Fig. 1c). Note that the 'early' response relative to one saccade coincides in time with the 'late' response relative to the previous saccade. Most neurons participated in both phases of the response, although the relative amplitudes of the two peaks varied across cells. The late response was compatible with latencies expected in the avian visual system[38]. By contrast, the early response occurred largely before the chickadee fixated on the preferred target and started even before the head began to move.

What accounts for the early response? We first considered that it may be a visual response to the previous fixation. Whenever a chickadee successfully gazed at a target, its preceding fixation also tended to be slightly closer to that target (median amplitude of 39° for the saccade landing on the target versus 46° for the following saccade; Extended Data Fig. 1e). Therefore, a neuron selective for gazes towards one target might also have elevated firing in response to preceding gazes. However, we found that this type of tuning did not fully explain the data. Rather, firing during saccades was independently tuned to both the previous and next fixations (Fig. 3e). We confirmed this result using a linear mixed effects model that accounted for the distances of both the previous and the next fixation to the preferred target (Extended Data Fig. 8a). Even two saccades preceded by identical gaze fixations produced different firing rates, depending on the fixations that followed (Fig. 3f). We conclude that the early response is not purely visual; rather, it appears to be predictive of the upcoming gaze.

These results indicate an intriguing hypothesis: at the end of each gaze fixation, the hippocampus encodes both a prediction of what the bird is about to see and a response to what the bird just saw. In individual neurons, this pattern appears as a biphasic (early and late) response aligned with saccades towards the preferred target. Thanks to the closed-loop design of our task, we could try to separately influence these two responses. We analysed the response of each cell to its preferred gaze target. We compared saccades when the target site was rewarded (and the light cue turned on) to saccades when the same site was unrewarded (and the light cue remained off; Fig. 3g). In the early response, firing rates were identical between these two conditions. This was expected because the hippocampus had no a priori information about the upcoming light cue. By contrast, firing rates diverged in the late response, with higher rates in the light-on condition. We conclude that late in the fixation period, the hippocampus responds to visual stimuli. This late response can represent information beyond the location of the gaze target.

Next, we asked how hippocampal responses changed if the chickadee was able to predict the upcoming light cue. Instead of rewarding a random site in each trial, we implemented a blocked-trial task in three birds, in which the same site was rewarded for six trials in a row. Chickadees found the rewarded site more quickly during the repeated trials, indicating that they understood the structure of the task (Extended Data Fig. 1f). We found that in the blocked-trial task, firing rates diverged during the early response (Fig. 3h and Extended Data Fig. 8b). In other words, the early response was predictive of the light cue even before the chickadee gazed at the correct site.

After diverging in the early response, firing rates continued to separate during the late response. Here we aimed to disambiguate the bird's prediction from the actual reaction to the light cue. We included a small number of 'catch trials' in which the reward was omitted—that is, the chickadee expected the light to turn on, but the light actually remained off. The absence of the expected light cue suppressed neural activity; the late response was weaker in catch trials than in light-on trials. However, this response was still stronger than in those trials when the chickadee did not expect the light cue.

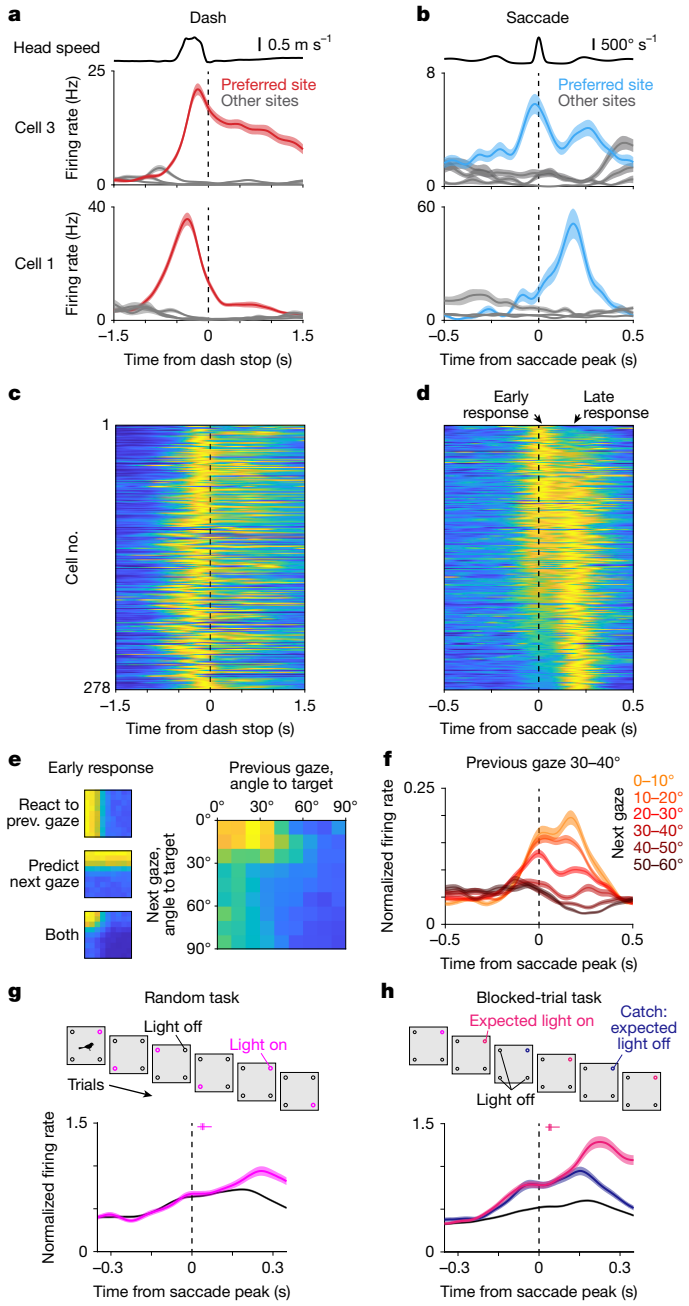

Fig. 3 | Gaze responses encode an internal prediction. a, Activity of two excitatory cells aligned to dashes towards each of the four target sites. Traces represent the mean ± s.e.m. across dashes. The average linear speed of the head across the entire dataset is shown above. **b**, Activity of the same two cells aligned to saccades towards the same four sites. Traces represent the mean ± s.e.m. across saccades. The average angular speed of the head is shown above. **c**, Activity of cells aligned to dashes towards their preferred target. Included are excitatory cells with strong selectivity (greater than 0.5) of both place and gaze responses for the same target. The activity of each cell is normalized from 0 (blue) to its maximum (yellow). **d**, Activity of the same cells aligned to saccades towards their preferred target. Cells are sorted by the difference in firing during the early and late phases of the response (centred on 17 and 187 ms); the same sorting was applied to **c**. **e**, Amplitude of the early response (at 17 ms relative to the saccade) in the same cells as in **c** and **d**, as a bivariate function of the distances to the target of the gazes that preceded and followed that saccade. Left, three hypotheses for what the bivariate function would look like if the early response is purely a reaction to the previous gaze, purely a prediction of the next gaze, or a function of both. Right, the actual data show that the early response is a function of both. Data are normalized firing rates averaged across neurons, from 0 (blue) to 0.17 (yellow). **f**, Responses to all saccades that were preceded by a gaze fixation 30–40° from the target, grouped by how far the next gaze landed from the target. These saccades correspond to the fourth column of the matrix in **e**. **g**, Responses to the preferred gaze target in the random task, separately for saccades when that target was correct (indicated by the light turning on) versus incorrect (indicated by the light staying off). Included are excitatory neurons with significant place and contralateral gaze tuning, peak firing rate above 1 Hz in the light-off condition and at least five saccades to the preferred gaze target (n = 271 cells); the activity of each cell is normalized to the peak rate during saccades in the light-off condition. Box and whisker: 5th, 25th, 50th, 75th and 95th percentiles of the latency to the light turning on (median = 40 ms). **h**, Responses to the preferred gaze target in the blocked-trial task, separately for saccades when the chickadee expected the target to turn on versus stay off (n = 402 cells; median latency to light on, 40 ms). Responses are also shown for catch trials, in which the target was expected to turn on but actually stayed off. In **f**–**h**, traces represent the mean ± s.e.m., averaged within a cell and then across cells.

In summary, activity during each saccade represents a mixture of information about the recently completed gaze fixation and a prediction about the upcoming fixation. We are unsure of what exactly the hippocampus predicted in our blocked-trial task: it could simply be the visual stimulus, or something more complex, such as reward anticipation. Regardless, the important conclusion is that the hippocampus represents both internally and externally driven information about visual targets. This coding is temporally coordinated by saccadic head movements, multiple times per second.

Inhibitory dynamics during saccades

The saccade-related dynamics that we observed are not unlike other fast phasic processes in the hippocampus, most notably the theta oscillation. Inhibition has a major role in these processes. For example, different classes of inhibitory interneurons fire at different phases of theta[39]. Such precise timing is thought to be important for the temporal patterning of excitatory cells and for the mechanisms of synaptic plasticity[40,41]. Birds do not appear to have continuous oscillations in the hippocampal local field potential[20]. We wondered whether their inhibitory and excitatory cells were instead temporally coordinated by head saccades.

As in previous studies[20,21,41], we classified chickadee hippocampal neurons as putative excitatory or inhibitory cells using firing rates and spike waveforms (Extended Data Fig. 9). Until this point, we have reported only the activity of excitatory cells; however, we now consider inhibitory cells. Our analysis revealed two types of gaze response in inhibitory cells. Some neurons (such as cell 1 in Fig. 4a) produced a smaller trough in firing shortly after the saccade and a larger peak in firing later during fixation. Other neurons (such as cell 2 in Fig. 4a) instead produced a smaller peak early and a larger trough later. We summarized these patterns by measuring the instantaneous phase of each cell's response at a fixed time after the saccade. Across the population, these phases had a clearly bimodal distribution, with two groups of cells roughly 180° apart (Fig. 4b–d). These groups ('peak' and 'trough' cells) also had different mean firing rates and spike waveforms (Fig. 4d and Extended Data Fig. 9). We conclude that peak and trough cells probably correspond to different classes of hippocampal interneurons.

Because saccades followed each other in quick succession, the firing rates of inhibitory cells contained several peaks (Fig. 4a–c). For example, peak cells produced the largest firing peak at 180 ms after the saccade. However, because the median inter-saccadic interval was approximately 270 ms (Fig. 1c), averaging across saccades produced several smaller versions of the same peak spaced by the inter-saccadic interval (such as at −90 and 450 ms). Owing to the multiple peaks, firing rates appeared to oscillate. Because saccades were irregularly timed, this was not a true periodic oscillation. Rather, the firing of inhibitory

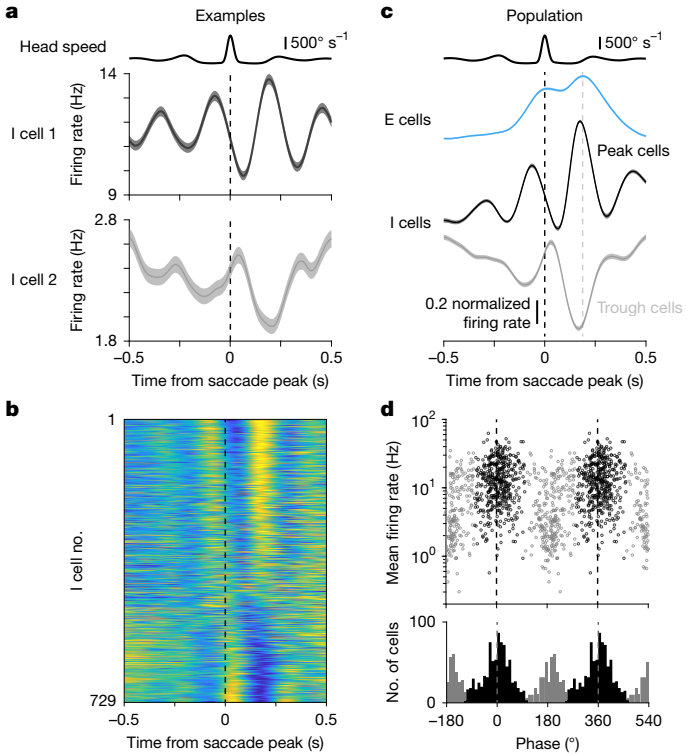

Fig. 4 | Inhibitory dynamics during saccades. a, Activity of two inhibitory (I) cells, averaged across all saccades regardless of target, otherwise plotted as in Fig. 3b. **b**, Responses of all I cells, sorted by the instantaneous Hilbert phase measured during the late response (at 187 ms). The response of each cell is normalized from minimum (blue) to maximum (yellow). **c**, Responses of excitatory (E) cells and two types of I cells (peak and trough), classified according to the phase at 187 ms. Dotted lines indicate 0 and 187 ms, the time of the second peak in excitatory cell firing. Traces represent the mean ± s.e.m., averaged within a cell and then across cells. **d**, Distribution of phases and mean firing rates (across the entire session) for all I cells. There is a clear bimodality of phases across the population.

cells should be considered a quasiperiodic oscillation entrained by saccades. In this oscillation, peak and trough cells fire out of phase with each other, and are both phase-shifted relative to excitatory cells. In summary, quasiperiodic saccade-related activity in chickadees has a major feature in common with theta oscillations in rodents: subtypes of interneurons that fire at different phases relative to each other and to the excitatory population.

Discussion

We have uncovered a critical role of vision in remotely driving place representations. Gaze responses in the hippocampus have previously been studied primarily in primates[10–15]. Considered without regard for place, chickadee hippocampal activity resembles responses in monkeys that also correlate with gaze location. Some of the primate hippocampal activity is invariant to the location of the animal, which is a property we demonstrated in chickadees using our all-to-all task. The similarity between birds and primates is notable because foveal vision in these species has evolved independently[4] and relies on different contributions of head and eye movement. Therefore, localized gaze responses seem to be fundamental to hippocampal function across these highly visual but phylogenetically distant species. Yet prior to our study, there was a major missing link between these gaze responses and the well-studied spatial representations in the hippocampus.

The main reason for this gap is that experimental primates are usually stationary, and technical challenges discourage their recording during movement. Only a few studies have managed to track gaze in navigating monkeys, either in virtual reality or with head-mounted devices[10,12–15]. These studies have not found the same close correspondence between place and gaze responses that we observed in chickadees. They also report only modest place and gaze selectivity compared to the robust firing fields in chickadees. One issue is sampling; in these studies, monkeys rarely viewed and visited the same locations—most gazes were at distal landmarks rather than the floor. Another issue is that much of the monkey gazing behaviour was passive rather than deliberately directed at spatial goals. By contrast, our visual search task forced chickadees to gaze directly at their navigational targets and ensured that these targets were behaviourally relevant. The motivational or attentional state could have a major effect on hippocampal signals. Finally, our task design separated periods of visual search from periods of navigation. Such an analysis proved to be critical because the coding of gaze and place was different during these non-overlapping periods of time. Future experimental designs and analyses may reveal more similarities between birds and primates.

Overlapping visual and spatial responses exist not only in the hippocampus, but also in the visual system itself. Experiments in owls have demonstrated place coding in parts of the visual hyperpallium[42]. Similar spatial activity was found in the primary visual cortex of mice[43]. These findings raise the question of where visual and spatial responses are computed. The hippocampal formation in both birds and mammals is strongly interconnected with the visual system[32–34]. It remains to be seen which features of neural activity arise in the hippocampus, which are inherited from the upstream visual regions, and whether the organization of these signals is conserved across species.

Our results also relate to remote activation of place cells in rodents. Hippocampal activity can encode places that are different from the rodent's actual location, both during rest[44] and during active behaviour[30,31]. Some remote activity during behaviour may be influenced by vision. For example, when navigating rats point their heads at distant targets, remote activity correlates with head direction[45,46]. Activity in the rodent hippocampal formation even encodes the angle of the eye relative to the head[47]. However, remote activity can also represent places behind the head or otherwise not visible to the animal, and therefore cannot be explained purely by vision[45]. A reasonable hypothesis is that vision at least partially affects hippocampal activity when rodents attend to distant visual targets. In most behaviours, testing this hypothesis is challenging because rodents lack a fovea and do not align their eyes precisely with visual targets[6,8,9]. However, in some behaviours such as hunting, the precise visual target is known[9]. Recordings during these behaviours will be informative for comparison with our results. Conversely, future work on birds will determine whether their remote activity is fully determined by gaze or whether, as in rodents, it can sometimes be unrelated to vision.

Another intriguing connection of our study is to theta oscillations. Theta is important for several types of temporal coding in the hippocampus. In rodents, different molecular and morphological classes of interneurons fire at different phases of theta[39]. Their timing is essential for coordinating the firing of excitatory cells and for mechanisms of synaptic plasticity[40,41]. In each theta cycle, the hippocampus switches between states dominated by external inputs and internal connections[48]. This process may enable the hippocampus to fluctuate between different functions, such as memory storage during one phase of theta and memory recall during another phase. These theories of theta are hard to reconcile with the fact that other species lack or at least have greatly reduced theta[17,20,49]. We demonstrate a potential solution: temporal patterns of hippocampal activity can instead be paced by irregular saccades, forming a quasiperiodic oscillation. Animals may store and recall spatial memories (including food cache memories in chickadees) during specific phases of the saccadic cycle. This fluctuation could be coordinated by specialized subsets of inhibitory cells, potentially homologous to the inhibitory cells found in mammals.

Similar to how saccades synchronize hippocampal activity with incoming visual information, theta oscillations can synchronize activity with active sensory processes, such as whisking, sniffing and stepping[50–52]. Therefore, saccadic modulation and theta might be analogous processes, each adapted for the sensory behaviours of a particular animal species. Our results are consistent with those of a study on the hippocampal local field potential in bats, which is aperiodic[53]. They might also be consistent with primate data[17,54,55], although primates seem to retain some theta oscillations, in addition to saccades. In particular, monkey recordings have shown differential modulation of putative excitatory and inhibitory cells during saccades[15].

Chickadee data allow us to formulate a general idea about hippocampal function. We suggest that hippocampal activity encodes the place that is currently relevant to the animal. For ground-foraging rodents, this place is usually directly in front of their nose. For highly visual animals such as birds and primates, this place is usually at a distant visual target. In both cases, behaviour forces some exceptions: rodents temporarily attend to distant targets to make navigational choices, whereas a moving bird might attend to its current location. As a result, both local and remote coding are present in the hippocampus, although in amounts that vary across species and behavioural tasks. The strength of our visual foraging task is that it required chickadees to use both types of coding and switch between them at experimentally well-defined moments in time. Our results suggest how the hippocampus can simultaneously perform local functions, such as forming a new spatial memory when storing a nut, and remote functions, such as recalling that memory from afar.

Online content

Any methods, additional references, Nature Portfolio reporting summaries, source data, extended data, supplementary information, acknowledgements, peer review information; details of author contributions and competing interests; and statements of data and code availability are available at https://doi.org/10.1038/s41586-025-09101-z.

1. Meister, M. L. R. & Buffalo, E. A. Getting directions from the hippocampus: the neural connection between looking and memory. *Neurobiol. Learn. Mem.* **134**, 135–144 (2016).
2. O'Keefe, J. & Dostrovsky, J. The hippocampus as a spatial map. Preliminary evidence from unit activity in the freely-moving rat. *Brain Res.* **34**, 171–175 (1971).
3. Colgin, L. L., Moser, E. I. & Moser, M.-B. Understanding memory through hippocampal remapping. *Trends Neurosci.* **31**, 469–477 (2008).
4. Land, M. F. Eye movements of vertebrates and their relation to eye form and function. *J. Comp. Physiol. A* **201**, 195–214 (2015).
5. Kane, S. A. & Zamani, M. Falcons pursue prey using visual motion cues: new perspectives from animal-borne cameras. *J. Exp. Biol.* **217**, 225–234 (2014).
6. Wallace, D. J. et al. Rats maintain an overhead binocular field at the expense of constant fusion. *Nature* **498**, 65–69 (2013).
7. Payne, H. L. & Raymond, J. L. Magnetic eye tracking in mice. *eLife* **6**, e29222 (2017).
8. Meyer, A. F., O'Keefe, J. & Poort, J. Two distinct types of eye-head coupling in freely moving mice. *Curr. Biol.* **30**, 2116–2130.e6 (2020).
9. Michaiel, A. M., Abe, E. T. & Niell, C. M. Dynamics of gaze control during prey capture in freely moving mice. *eLife* **9**, e57458 (2020).
10. Rolls, E. T., Robertson, R. G. & Georges-François, P. Spatial view cells in the primate hippocampus. *Eur. J. Neurosci.* **9**, 1789–1794 (1997).
11. Killian, N. J., Jutras, M. J. & Buffalo, E. A. A map of visual space in the primate entorhinal cortex. *Nature* **491**, 761–764 (2012).
12. Wirth, S., Baraduc, P., Planté, A., Pinède, S. & Duhamel, J.-R. Gaze-informed, task-situated representation of space in primate hippocampus during virtual navigation. *PLoS Biol.* **15**, e2001045 (2017).
13. Mao, D. et al. Spatial modulation of hippocampal activity in freely moving macaques. *Neuron* **109**, 3521–3534.e6 (2021).
14. Corrigan, B. W. et al. View cells in the hippocampus and prefrontal cortex of macaques during virtual navigation. *Hippocampus* **33**, 573–585 (2023).
15. Piza, D. B. et al. Primacy of vision shapes behavioral strategies and neural substrates of spatial navigation in marmoset hippocampus. *Nat. Commun.* **15**, 4053 (2024).
16. Fried, I., MacDonald, K. A. & Wilson, C. L. Single neuron activity in human hippocampus and amygdala during recognition of faces and objects. *Neuron* **18**, 753–765 (1997).
17. Jutras, M. J., Fries, P. & Buffalo, E. A. Oscillatory activity in the monkey hippocampus during visual exploration and memory formation. *Proc. Natl Acad. Sci. USA* **110**, 13144–13149 (2013).
18. Gulli, R. A. et al. Context-dependent representations of objects and space in the primate hippocampus during virtual navigation. *Nat. Neurosci.* **23**, 103–112 (2020).
19. Moore, B. A., Doppler, M., Young, J. E. & Fernández-Juricic, E. Interspecific differences in the visual system and scanning behavior of three forest passerines that form heterospecific flocks. *J. Comp. Physiol. A* **199**, 263–277 (2013).
20. Payne, H. L., Lynch, G. F. & Aronov, D. Neural representations of space in the hippocampus of a food-caching bird. *Science* **373**, 343–348 (2021).
21. Chettih, S. N., Mackevicius, E. L., Hale, S. & Aronov, D. Barcoding of episodic memories in the hippocampus of a food-caching bird. *Cell* **187**, 1922–1935.e20 (2024).
22. Martin, G. R., White, C. R. & Butler, P. J. Vision and the foraging technique of Great Cormorants *Phalacrocorax carbo*: pursuit or close-quarter foraging? *IBIS* **150**, 485–494 (2008).
23. Theunissen, L. M. & Troje, N. F. Head stabilization in the pigeon: role of vision to correct for translational and rotational disturbances. *Front. Neurosci.* **11**, 551 (2017).
24. Bischof, H.-J. The visual field and visually guided behavior in the zebra finch (*Taeniopygia guttata*). *J. Comp. Physiol. A* **163**, 329–337 (1988).
25. Maldonado, P. E., Maturana, H. & Varela, F. J. Frontal and lateral visual system in birds: frontal and lateral gaze. *Brain Behav. Evol.* **32**, 57–62 (2008).
26. Itahara, A. & Kano, F. Gaze tracking of large-billed crows (*Corvus macrorhynchos*) in a motion capture system. *J. Exp. Biol.* **227**, jeb246514 (2024).
27. Wilson, M. A. & McNaughton, B. L. Dynamics of the hippocampal ensemble code for space. *Science* **261**, 1055–1058 (1993).
28. Anderson, M. I. & Jeffery, K. J. Heterogeneous modulation of place cell firing by changes in context. *J. Neurosci.* **23**, 8827–8835 (2003).
29. Aronov, D., Nevers, R. & Tank, D. W. Mapping of a non-spatial dimension by the hippocampal–entorhinal circuit. *Nature* **543**, 719–722 (2017).
30. Pfeiffer, B. E. & Foster, D. J. Hippocampal place-cell sequences depict future paths to remembered goals. *Nature* **497**, 74–79 (2013).
31. Kay, K. et al. Constant sub-second cycling between representations of possible futures in the hippocampus. *Cell* **180**, 552–567.e25 (2020).
32. Felleman, D. J. & Van Essen, D. C. Distributed hierarchical processing in the primate cerebral cortex. *Cereb. Cortex* **1**, 1–47 (1991).
33. Atoji, Y. & Wild, J. M. Projections of the densocellular part of the hyperpallium in the rostral Wulst of pigeons (*Columba livia*). *Brain Res.* **1711**, 130–139 (2019).
34. Applegate, M. C., Gutnichenko, K. S. & Aronov, D. Topography of inputs into the hippocampal formation of a food-caching bird. *J. Comp. Neurol.* **531**, 1669–1688 (2023).
35. Zeigler, H. P. & Bischof, H.-J. *Vision, Brain, and Behavior in Birds* (MIT Press, 1993).
36. Sherry, D. F., Krebs, J. R. & Cowie, R. J. Memory for the location of stored food in marsh tits. *Anim. Behav.* **29**, 1260–1266 (1981).
37. Graves, J. A. & Goodale, M. A. Failure of interocular transfer in the pigeon (*Columba livia*). *Physiol. Behav.* **19**, 425–428 (1977).
38. Gusel'nikov, V. I., Morenkov, E. D. & Hunh, D. C. Responses and properties of receptive fields of neurons in the visual projection zone of the pigeon hyperstriatum. *Neurosci. Behav. Physiol.* **8**, 210–215 (1977).
39. Klausberger, T. et al. Brain-state- and cell-type-specific firing of hippocampal interneurons in vivo. *Nature* **421**, 844–848 (2003).
40. Mehta, M. R., Lee, A. K. & Wilson, M. A. Role of experience and oscillations in transforming a rate code into a temporal code. *Nature* **417**, 741–746 (2002).
41. Mizuseki, K., Sirota, A., Pastalkova, E. & Buzsáki, G. Theta oscillations provide temporal windows for local circuit computation in the entorhinal–hippocampal loop. *Neuron* **64**, 267–280 (2009).
42. Agarwal, A., Sarel, A., Derdikman, D., Ulanovsky, N. & Gutfreund, Y. Spatial coding in the hippocampus and hyperpallium of flying owls. *Proc. Natl Acad. Sci. USA* **120**, e2212418120 (2023).
43. Saleem, A. B., Diamanti, E. M., Fournier, J., Harris, K. D. & Carandini, M. Coherent encoding of subjective spatial position in visual cortex and hippocampus. *Nature* **562**, 124–127 (2018).
44. Wilson, M. A. & McNaughton, B. L. Reactivation of hippocampal ensemble memories during sleep. *Science* **265**, 676–679 (1994).
45. Johnson, A. & Redish, A. D. Neural ensembles in CA3 transiently encode paths forward of the animal at a decision point. *J. Neurosci.* **27**, 12176–12189 (2007).
46. Ormond, J. & O'Keefe, J. Hippocampal place cells have goal-oriented vector fields during navigation. *Nature* **607**, 741–746 (2022).
47. Mallory, C. S. et al. Mouse entorhinal cortex encodes a diverse repertoire of self-motion signals. *Nat. Commun.* **12**, 671 (2021).
48. Hasselmo, M. E., Bodelón, C. & Wyble, B. P. A proposed function for hippocampal theta rhythm: separate phases of encoding and retrieval enhance reversal of prior learning. *Neural Comput.* **14**, 793–817 (2002).
49. Yartsev, M. M., Witter, M. P. & Ulanovsky, N. Grid cells without theta oscillations in the entorhinal cortex of bats. *Nature* **479**, 103–107 (2011).
50. Macrides, F., Eichenbaum, H. B. & Forbes, W. B. Temporal relationship between sniffing and the limbic theta rhythm during odor discrimination reversal learning. *J. Neurosci.* **2**, 1705–1717 (1982).
51. Grion, N., Akrami, A., Zuo, Y., Stella, F. & Diamond, M. E. Coherence between rat sensorimotor system and hippocampus is enhanced during tactile discrimination. *PLoS Biol.* **14**, e1002384 (2016).
52. Joshi, A. et al. Dynamic synchronization between hippocampal representations and stepping. *Nature* **617**, 125–131 (2023).
53. Eliav, T. et al. Nonoscillatory phase coding and synchronization in the bat hippocampal formation. *Cell* **175**, 1119–1130.e15 (2018).
54. Hoffman, K. et al. Saccades during visual exploration align hippocampal 3–8 Hz rhythms in human and non-human primates. *Front. Syst. Neurosci.* **7**, 43 (2013).
55. Andrillon, T., Nir, Y., Cirelli, C., Tononi, G. & Fried, I. Single-neuron activity and eye movements during human REM sleep and awake vision. *Nat. Commun.* **6**, 7884 (2015).

Publisher's note Springer Nature remains neutral with regard to jurisdictional claims in published maps and institutional affiliations.

Springer Nature or its licensor (e.g. a society or other partner) holds exclusive rights to this article under a publishing agreement with the author(s) or other rightsholder(s); author self-archiving of the accepted manuscript version of this article is solely governed by the terms of such publishing agreement and applicable law.

© The Author(s), under exclusive licence to Springer Nature Limited 2025

Methods

Subjects

All animal procedures were approved by the Columbia University Institutional Animal Care and Use Committee and performed in accordance with the guidelines of the US National Institutes of Health. The subjects were nine adult black-capped chickadees (*Poecile atricapillus*) collected from several sites in New York State using federal and state scientific collection permits. Of these, eight birds (five males and three females) were used for neural recordings (seven in the random task, three in the blocked-trial task and three in the all-to-all task), and some birds were used in multiple tasks. The ninth bird (male) was used to measure the accuracy of eye tracking. Experiments were conducted blind to sex because chickadees do not have noticeable sexual dimorphism. Sex was determined after experiments were completed. During the experiments, the birds were singly housed on a 'winter' light cycle (9 h:15 h light:dark). The primary wing feathers were trimmed to prevent flight.

Head tracking and gaze estimation

To determine whether gaze could be estimated from head movements alone and to estimate the direction of that gaze, we first conducted behaviour-only calibration sessions for each bird. During calibration, the bird sat on a single perch, and both head and eye movements were measured simultaneously (Fig. 1). For these sessions, we used the same behavioural arena as for the full task described below, but the floor was configured with a single perch near a dish of seed fragments to encourage perching in one place.

Head position was tracked using an infrared-based motion capture system (Qualisys Miqus cameras and Qualisys Track Manager software) consisting of four specialized infrared cameras recording at 300 frames s^{-1}. The motion capture system tracked a three-dimensional (3D)-printed arrangement ('rigid body') of five reflective markers (3M Scotchlite 7610 Reflective Tape) affixed to an implant on the bird's head using neodymium magnets and a 3D-printed kinematic mount (Fig. 1a). We calculated the position of the rigid body in the 'world' reference frame anchored by known landmarks in the arena.

Eye position was tracked using a custom dual-camera video-oculography system based on existing techniques that do not require the cooperation of the subject for calibration[56,57]. The video-oculography system consisted of two cameras positioned 4 cm apart (Blackfly S BFS-U3-27S5M; Edmund Optics 59871 25 mm/F1.4 lens; visible light-blocking filter) and two infrared light sources positioned 11 cm apart (850 nm; Mouser 416-LST101H01IR0101). All cameras and light sources were aimed at the bird sitting on the perch.

Before eye position could be recorded, a three-step process was used to calibrate the combined head and eye tracking system. First, we determined the relative positions of the two cameras and their lens parameters using a chequerboard grid and the MATLAB computer vision toolbox (R2021a). This step defined a 'video-oculography' reference frame centred on the optical centre of the first camera. Second, we determined the positions of the infrared light sources relative to the video-oculography reference frame by imaging their reflections in a front surface mirror. The position and orientation of the mirror plane were determined using a chequerboard affixed to its mirrored surface. Finally, we aligned the world and video-oculography reference frames by determining the position of an arrangement of three reflective markers simultaneously in both systems.

For every frame in which the eye was visible in both video-oculography cameras, we used a published algorithm[58] to determine the pixel coordinates of the pupil and the reflections of the two infrared light sources on the corneal surface. Using the camera calibration described above, we converted the two-dimensional pixel coordinates to 3D positions in the video-oculography reference frame. Finally, we estimated the centre of corneal curvature using the positions of the two corneal reflections and the positions of the infrared light sources relative to the eye and cameras. We defined the position of the eye as the centre of corneal curvature, and defined the optical axis of the eye as the vector pointing from the centre of corneal curvature to the pupil centre. MATLAB code for the eye tracking calibrations and analysis is available at https://github.com/hpay/eyetrack-bird. We applied several quality checks to discard frames in which the eye tracking failed.

We next defined a 'head'-centred reference frame, which was applied to the calibration session and to all experimental sessions. The position of the head (origin) was taken as the midpoint of the two eyes, averaged across frames. The *x* axis passed through the two eyes (right positive), the *y* axis passed through the midpoint of the two eyes and the tip of the beak (beak positive) and the *z* axis pointed up. We determined the orientation of the eye relative to the head in this reference frame. In Fig. 1d, we subtracted the mean horizontal and vertical angles of the eye from each data point to show the range of eye movements from rest. For the discrete visual search task described below, we used the mean position and vector of each eye in the head-centred reference frame to estimate the directions of gaze.

Accuracy of head and eye tracking

To measure the accuracy of head tracking, we mounted the same rigid body of five markers that we used in the experiments onto a motorized rotation stage (Physik Instrumente M-660.45). We placed the stage inside the experimental arena and rotated the rigid body in 1° increments. For each angle, we measured the average orientation of the rigid body over 330 ms of tracking data (to match a typical duration of a head fixation). We compared this orientation with the actual rotation of the motorized stage (Extended Data Fig. 2b). We also measured the translational error of each individual marker's position, relative to the fit of all markers to the rigid body, as provided by the Qualisys Track Manager software (0.22 mm; mean residual).

To measure the accuracy of eye tracking, we mounted a recently euthanized chickadee onto the motorized rotation stage. We opened one of the eyelids and kept the eye wet with saline. We placed the rotation stage in front of the video-oculography camera set-up described above. We rotated the chickadee in 1° increments and used the same analyses to track the eye as we did in our calibration experiments. We compared the orientation of the eye with the actual rotation of the motorized stage (Extended Data Fig. 2c).

Behavioural experiments

All experiments were conducted in an enclosed square arena, with a central open space of 61 cm on each side, surrounded by a 2.5-cm boundary interrupted by corner posts. The walls, floor and ceiling were black, with approximately 15-cm-diameter bright shapes (yellow circle, pink star, blue pentagon and green tree) positioned on each wall and centred approximately 30 cm above the floor. The arena was illuminated from above. White noise was played in the background to mask inadvertent room noise.

Five feeder modules were positioned in the configurations described below for each task. Each module consisted of three concentric circles: a 3D-printed perch (50-mm outer diameter, 30-mm inner diameter and 6.25-mm total height above the arena floor), surrounding a raised ring of light-emitting diodes (eight DotStar light-emitting diodes per ring; Adafruit Industries) mounted on a custom printed circuit board behind a diffuser (19 mm outer diameter, 13 mm inner diameter and 5.25-mm height above the arena floor) and surrounding a motorized feeder (11.6-mm opening diameter) that dispensed tiny sunflower seed fragments (approximately 1.5 mg each) from a cup (4-mm deep). This arrangement ensured that the bird could not see into the feeder from a different perch, given a vertical head position of 54 ± 6 mm (mean ± s.d.; $n = 58$ sessions).

In the random and blocked-trial tasks described below, the bird was encouraged to remain on the paths between the central and outer

perches by a rubber surface restricted to an X shape, with each arm measuring 7.5 cm in width. The rest of the arena was covered with a slippery ultra-high-molecular-weight polyethylene surface. For the all-to-all task, the rubber surface covered the entire arena, but birds still preferred to hop directly between perches.

To motivate food consumption, birds were deprived of food for 1–3 h from waking (at the beginning of the light-on period of the day) until the start of the experiment. Birds were weighed daily before the experiment to ensure stable weight. Sessions typically lasted 1 h. Birds typically underwent three to six habituation sessions, some conducted before surgery and some afterwards. Wired electrophysiological recordings began after these sessions. The weight from the implanted recording device and cable was partially offset by a thin strand of fibre extracted from an elastic string (Linsoir Beads; Crystal String).

The light and feeder states were controlled in real time by the animal's behaviour. We tracked behaviour at 300 frames s^{-1} using the reflective head markers and the calibrated motion capture system described above. The head marker coordinates were streamed from Qualisys Track Manager to MATLAB using the software interface QTM Connect for MATLAB (Qualisys AB). The saved calibrations for each bird were then used to determine the head position and gaze vectors for each eye. In preliminary behavioural experiments, we found that birds typically directed their gaze towards targets along a vector slightly below the optical axis of the eye (Fig. 1h, left). Therefore, we rotated the estimated gaze vectors for each eye downwards by 5° during real-time tracking. The bird's behaviour controlled the experimental flow using the MATLAB code, as described in detail below. Finally, MATLAB sent serial commands to an Arduino Mega to change the light and feeder states.

In all tasks, seed retrieval was detected when the bird's beak tip was within 1 cm of the centre of the site, increasing to 8 cm when the light was on but the feeder was closed. During pretraining of uncalibrated birds, detection occurred when the bird's head was within 5 cm of the site. The feeder remained open for a fixed time (T_{open}). We gradually reduced T_{open} from 20 to 1–2 s during pretraining, with the exact value chosen such that each bird had enough time to make only one beak poke. After T_{open}, the feeder was closed and the light was turned off. Feeder opening and closing occurred smoothly over a total duration of 1 s.

In the random task, five identical sites were arranged in an X shape. Each outer site was 34 cm from the central site. In this task, every session started with the central site ('centre') illuminated ('turned on') and its feeder open. Next, one of the four outer target sites was pseudorandomly selected as the rewarded 'target' site. We ensured that the same site was never chosen twice in a row, and that each site was chosen a roughly equal number of times per session. During some pretraining sessions (Fig. 1g), the target turned on after a random delay (no more than 5 s). For the remaining experimental sessions, the target only turned on when the bird was sitting at the centre and gazing towards the target within a threshold of 10–20° of angular deviation for at least three time points. The median latency from the time of peak saccade velocity to the time of light onset was 40 ms (n = 8,973 trials; Fig. 3e), and the median time to fixation onset was 33 ms. Both eyes could trigger the target to turn on. If the bird visited any outer site before triggering the correct target with gaze, the centre turned on and the programme waited for the bird to return to the centre. The target light turned on every time the gaze trigger was activated.

After the target site turned on, there were two variants of what happened next. In the 'stable' variant of the task, the target stayed on until the bird visited the feeder. In the 'transient' variant, the target only remained on while gaze was fixated at the target, but it turned on again when the bird approached the site (within 8 cm). For the random task, both task variants were used and pooled because the analyses did not depend on the state of the light after initial detection. For the blocked-trial task, all sessions were transient. For the all-to-all task, which was more difficult for the birds to learn, all sessions were stable.

After the target turned on, the programme waited for the bird to visit the target and, if the feeder opened, retrieve a seed. The feeder was opened with a probability chosen manually on the basis of the bird's behaviour (50–100%) to maintain motivation and increase the number of trials. Incorrect site visits were indicated by turning the target off and the centre on and requiring the bird to visit the centre before the target turned on again. When the bird successfully retrieved a seed from the target feeder, the target turned off and the centre turned on (with a low probability of reward, 5–25%). We considered a single trial to consist of one correct outward dash towards the target and one inward dash towards the centre. Thus, this task elicited self-paced but structured centre-out visual search behaviour, with many dashes and saccades towards the same four outer sites.

The blocked-trial task (Fig. 3f) had an identical physical arrangement. By contrast to the random task, the target was not chosen randomly but instead was repeated six times in a row. For the first trial in a block, the target always turned on every time the bird's gaze was directed towards the target. To increase the number of trials in each condition, only the contralateral eye could trigger gaze in this task. (For birds that were trained on both the random and blocked-trial tasks, the blocked-trial task was always run after the random task to avoid introducing any bias in eye usage in the random task). For the second to sixth trials in a block, two of the trials were pseudorandomly chosen as 'catch' trials. During a catch trial, the target remained off the first time the bird's gaze was directed at the target. In all subsequent gaze detections, the target turned on. The catch trials were balanced such that, over a session, there was nearly an equal number (±1) of catch trials at each position within a block. In this task, the median latency from peak saccade velocity to fixation onset was 33 ms, whereas the median latency to from peak saccade velocity to light onset was 40 ms, similar to the random task.

The all-to-all task (Extended Data Fig. 3) had five sites arranged in a pentagon. There was no centre site, and the targets were chosen pseudorandomly in an all-to-all order. Sequences requiring the bird to visit three adjacent sites in a row were excluded from the pseudorandom assignment, and target pair counts were balanced within a session. Incorrect visits were indicated by turning off the current target and turning on the previous target, requiring the bird to return to the previous site before activating a gaze trigger or feeder opening. Both eyes could trigger the target to turn on.

Electrophysiological recording

We developed a lightweight system for chronic recording during free behaviour[21]. Neural activity was recorded using a 64-channel silicon neural probe (Cambridge NeuroTech; H5 or H6 ASSY-236). A three-part 3D-printed housing system secured the headstage and protected the probe.

Signals were amplified, multiplexed and digitized at 30,000 Hz using a custom printed circuit board containing a wire-bonded RHD2164 chip (Intan Technologies). Intan RHX Data Acquisition Software (Intan Technologies) recorded the neural data simultaneously with the time of each video frame from the head tracking system and the times of light or feeder changes from the behavioural control system. Digital signals were transmitted from the bird to a computer interface board through a 12-conductor SPI cable (Intan Technologies; C3213) and passed through a motorized commutator (Doric Lenses; AERJ_24_HDMI).

To minimize the degradation of neural signals over time, the probe contacts were left embedded in a silicone gel covering the brain when not in use. The probe was inserted to the desired depth 30 min before recording and retracted at the end of each session using an aluminium nanodrive (Cambridge NeuroTech).

The entire assembly was 1.1 g (0.1 g probe, 0.40 g headstage and connectors, 0.28 g drive and 0.32 g housing). The addition of cement increased the weight by approximately 0.2 g, and the rigid body of reflective markers added an extra 0.14 g.

Surgery

Surgery was performed using a two-step procedure, as described in a previous study[21]. First, a dummy implant with a removable cap was affixed to the skull. The bird was allowed to recover, and removable weights were gradually added. Second, craniotomy was performed, and the probe was implanted.

During the first step, the bird was anaesthetized using 1.5% isoflurane in oxygen. Feathers were removed from the surgical site, and the bird was placed in a modified stereotaxic apparatus using ear bars and a beak clamp. The head was tilted such that the angle of the groove at the base of the upper mandible of the beak was 65° relative to the horizontal, corresponding to an angle of 30° between the bite bar and the horizontal. A silver ground wire (0.005-in. diameter) was implanted in the contralateral hemisphere, posterior and lateral to the hippocampus and 1 mm below the surface. The location of the probe craniotomy was marked on the surface of the skull: 3.02–4.05 mm anterior to lambda and 0.5–0.73 mm lateral to the midline. Most microdrives were implanted in the left hippocampus, with two microdrives implanted in the right hippocampus. The tilt of the head was adjusted so that the 3D-printed base would sit flat on the skull when centred over the craniotomy. A short base unit was cemented over the planned craniotomy (3M RelyX Unicem). A removable 3D-printed cap was attached to the base unit. After the surgery, buprenorphine (0.05 mg kg^{-1}) was injected intraperitoneally, and the bird was allowed to recover for 1.5–2 weeks while weight was monitored. After at least 5 days, a 1-g weight was added to the dummy cap.

During the second step, the bird was anaesthetized as described above and injected intraperitoneally with dexamethasone (2 mg kg^{-1}). The cap of the dummy implant was removed, and the remaining base unit and skull were cleaned with 70% ethanol. A craniotomy and durotomy were performed covering a 1 × 1 mm area centred on the coordinates given above. A 3D-printed biocompatible resin insert with a small central slit (0.4 × 0.1 mm) was inserted into the craniotomy site so that it pressed gently on the brain surface and was cemented to the skull. A silicon probe mounted on a drive was then moved into place and tilted laterally by 10–15° to target the medial hippocampus. After checking the insertion of the probe, the space above the craniotomy was filled with a protective layer of silicone elastomer (Dow Corning 3-4680 Silicone Gel). The probe was advanced to sit in the elastomer, and the drive was cemented into place. The protective outer housing and headstage were secured over the probe. The top surface of the outer housing contained a hole to access the drive screw, and a kinematic mount composed of two small neodymium magnets and 3D-printed features to allow reliable repositioning of the reflective markers during behavioural sessions.

Histology

After completion of all experiments for each bird, the silicon probe was left in place overnight. The bird was given an overdose of ketamine and xylazine and was then perfused transcardially with saline followed by 4% formaldehyde. Brains were extracted and stored in 4% formaldehyde and then cut into 100-µm-thick coronal sections. Brain sections were stained with fluorescent 4′,6-diamidino-2-phenylindole (DAPI). The position of each electrode relative to the boundary of the hippocampus was estimated by measuring the distance from the surface of the brain to the lateral ventricle along the electrode track. This measurement was used to exclude recorded cells that were probably outside the hippocampus.

Spike sorting

All analyses were conducted in MATLAB unless otherwise noted. Spike sorting was conducted using Kilosort v.2.0 (ref. 59). Default settings were used, except that the high-pass filtering cut-off was set to 300 Hz, and there was no minimum firing rate for good channels. A total of 25 sessions were manually curated in Phy (Python), including 15 in the current dataset and ten from previous pilot experiments. During manual curation, the automatic labels were edited as needed to mark units as 'good', 'mua' (multi-unit activity) and 'noise'. The remaining 55 sessions were automatically curated by applying several criteria.

First, we calculated the spatial extent of each unit along the probe, as well as the cluster contamination rate determined by Kilosort, and excluded units that passed a threshold for each.

Second, we identified putative excitatory and inhibitory neurons by applying a Gaussian mixture model (GMM) to the following four electrophysiological characteristics (Extended Data Fig. 5): spike rate (log-transformed), spike width, spike asymmetry and derivative peak–trough ratio. Spike width was calculated as the time from the trough of the average spike waveform to the subsequent peak. Spike asymmetry was calculated as the relative height of the two positive peaks flanking the trough. Derivative peak–trough ratio was the log-transformed ratio of the peak amplitude to the trough amplitude of the waveform derivative. We fitted the GMM on the manually curated sessions to classify cells into two clusters corresponding to putative excitatory and inhibitory neurons. We then applied the GMM to all sessions and excluded units that exceeded a distance threshold from either of the two clusters. A small number of neurons that were intermediate between the two clusters were labelled as unclassified neurons and were not considered further. Cells with fewer than 500 spikes were excluded (457 of 3,115 cells). The code to run spike sorting and process results is available at https://github.com/hpay/spikesort-hp-2025.

Inhibitory neurons were further clustered into two groups on the basis of their average saccade-aligned activity (Fig. 4). The mean firing rates were 1.3, 14.0 and 7.1 Hz in the putative excitatory, late inhibitory and early inhibitory clusters, respectively. The spike widths were 0.51, 0.27 and 0.33 ms, respectively. The peak amplitude asymmetries were −0.04, 0.55 and 0.56.

Behavioural analysis

The position and orientation of the head were tracked using the motion capture system, as described above. The linear head speed was calculated by differentiating the x, y and z positions of the head and calculating the absolute speed as $\sqrt{\Delta x^2 + \Delta y^2 + \Delta z^2}/\Delta t$. The angular head speed was calculated by measuring the angular difference in the 3D orientation of the head between adjacent frames and dividing it by Δt. Both linear and angular speeds were then low-pass filtered using a Butterworth filter with a cut-off frequency of 25 Hz.

Hidden Markov model. To label the behavioural states, we implemented an HMM based closely on a previous study[60]. The HMM predicted whether the bird was saccading, fixating or feeding at each of the five sites, or whether it was dashing between two pairs of sites. The HMM had a Gaussian observation model, representing the likelihood of observing the position, orientation and speed of the bird's head at each time point given each state. The most probable state was computed using the Viterbi algorithm. The input data consisted of linear speed, angular speed, head position and head tilt. Head position was transformed to represent proximity to the sites or lines between sites. The mean parameters of the Gaussian model were fitted iteratively for each session, whereas the variance parameters were fixed. The transition probability matrix was fixed.

We refined the HMM output as follows. First, misclassified states were corrected. Any 'saccades' immediately preceding feeding were combined with the feeding state. Any 'saccades' immediately following a dash were combined with the dash state. Any 'feeding' after a dash was combined with the dash. Second, we refined the end points of the saccades and dashes. The start and stop times of each saccade were refined by applying velocity (400° s^{-1}) and acceleration (5,000° s^{-2}) thresholds. The stop time of each dash was also refined by applying velocity (150 mm s^{-1}) and acceleration (3,000 mm s^{-2}) thresholds.

Sessions with fewer than five dashes or five saccades with each eye to each outer site were excluded from further analyses. Unless otherwise noted, all analyses were conducted on saccades that were immediately followed by a fixation. We used the time of peak saccade velocity as the alignment point for all analyses (the 'time of the saccade').

Analysis of gaze strategies. To calculate the time course of gaze strategies shown in Fig. 1g and Extended Data Fig. 1d, a histogram of head orientations relative to the target was first calculated for each bird, and the peak density near the beak and near each eye (averaged across eyes) was taken as the ideal vector for the frontal and lateral gazes, respectively. For each saccade in the sequence, we then determined the angular distance between either frontal gaze or lateral gaze with either eye and the target of the upcoming dash. Angular distances less than 20° were counted as 'hits', and the probability of a hit for either frontal or lateral gaze across all saccades was plotted.

Neural analysis

Place and gaze responses. To construct place map examples (Fig. 2c), we included position data during dashes plus a ±1 s window before and after each dash. Spatial information was calculated using a range of delays between spikes and behaviour, and the best offset was chosen. The arena floor was divided into 40 × 40 bins in which spike counts and occupancy time were calculated. The resulting matrices were smoothed with an 11 × 11-point Hamming window and then divided to yield the mean firing rate.

The gaze maps (Fig. 2d) included data during gaze fixations made while at the centre site. Gaze from the specified eye was projected along the optical axis measured during the calibration session from that bird. A cone with a radius of 10° was projected on the floor. Spike counts and occupancy times were calculated, smoothed with a 9 × 9-point Hamming window and divided to yield the mean firing rate in each bin.

We quantified the degree of spatial tuning for each neuron for both place and gaze. We quantified place tuning by calculating the information about site identity conveyed by the cell's firing during dashes towards each of the four outer sites. We calculated this information according to:

$$I = \sum_x \frac{\lambda(x)}{\lambda} \log_2 \frac{\lambda(x)}{\lambda} p(x)$$

where I is the information rate in bits per spike, $x \in \{1,2,3,4\}$ is the site identity, $p(x)$ is the probability that the bird visited site x, $\lambda(x)$ is the mean firing rate in a ±1 s window centred at the end of each dash to site x, and $\lambda = \Sigma\lambda(x)p(x)$ is the overall mean firing rate across all included time periods[61]. A null distribution for each cell was calculated by shuffling the identity of the dash targets across trials and recalculating the spatial information for 200 repetitions. A neuron was considered a significant 'place cell' if the actual spatial information exceeded 99% of the samples in the shuffled distribution. The spatial information was normalized for each cell by dividing the actual spatial information by the mean of the shuffled distribution (Fig. 1g).

We applied the same procedure to quantify the degree of gaze tuning but for spike counts within a window from −0.1 to +0.3 s from the time of peak saccade velocity. Only saccades that landed on a target (within 20° of visual angle) and that occurred more than 0.5 s before the start of a dash were included.

Firing rates were calculated over time by binning spikes at the frequency of the behavioural data acquisition (3.33-ms bins) and applying either a 100-ms or a 30-ms sigma Gaussian filter for dash or gaze responses, respectively.

Dash responses were summarized across the population (Fig. 2e) by calculating the average firing rate over time aligned to dashes to each of the four outer sites for each neuron. The peak of the response in a ±1 s window centred on the dash end was measured for each of the four sites. Saccade responses were summarized across the population (Fig. 2f) using a different approach, because the configuration of sites (separated by 90°) resulted in behavioural correlations between gazes with each eye to adjacent sites (angle between eyes 106 ± 5°; mean ± s.d.; $n = 8$ birds). We estimated the separate contributions of ipsiversive and contraversive gaze to neural firing using a Poisson generalized linear model. Lasso regression was applied using the MATLAB function lassoglm with $\alpha = 1$ and $\lambda = 0.005$ to prevent overfitting. The model was given by:

$$\log(E(\mathbf{y}|\mathbf{X})) = \boldsymbol{\beta}'\mathbf{X}$$

where each element of $\mathbf{y}$ is a scalar y_i containing the observed spike count within a window from −0.1 s before to +0.3 s after the time of peak saccade velocity for trial i. Each column of $\mathbf{X}$ contained the predictors $\mathbf{x}_i$, which are given by:

$$\mathbf{x}_i = e^{-\frac{\boldsymbol{\alpha}^2}{\tau^2}}$$

where $\boldsymbol{\alpha}$ is a vector representing the angular distance of each site from each eye's gaze vector, contralateral (C) or ipsilateral (I) to the site of recording:

$$\boldsymbol{\alpha} = [\alpha_C^1\ \alpha_C^2\ \alpha_C^3\ \alpha_C^4\ \alpha_I^1\ \alpha_I^2\ \alpha_I^3\ \alpha_I^4]$$

and τ is a length constant equal to 45°, determined by fitting the decay of neural activity across the population as a Gaussian function of distance.

For the all-to-all task, birds started each trial in a different location, so place codes for a preferred site could contaminate responses during gaze from that site to other non-preferred sites. To account for this, we subtracted the baseline activity from both the dash and saccade responses in this task as follows. The neural response for dashes was calculated as the mean response in a ±0.5 s window centred on the dash end, minus the mean response from −2 to −1 s. The neural response for saccades was calculated as the mean response in a 0 to +0.3 s window aligned to the saccade minus the mean response from −1 to −0.2 s. Responses below zero were included in the analysis, but the colour plots were cropped at zero. All included cells had at least four saccades and four dashes for every source–target pair (20 total permutations).

We determined the selectivity of each cell for place or gaze at a single site by comparing responses for the preferred site to the next most preferred site. Responses for dash and gaze (either peak rates for dash or model coefficients for gaze) were first normalized by dividing by the response for the preferred site. A selectivity index was calculated as follows:

$$I_{\text{select}} = r_1 - r_2$$

where r_1 is the normalized response for the site with the largest response, and r_2 is the response for the site with the second largest response.

In Fig. 3c,d, cells are sorted by their difference in firing during the early and late responses relative to head saccades. To define the early and late responses, we calculated the mean firing aligned to saccades for each cell. We then averaged these responses across all excitatory cells with strong selectivity (greater than 0.5) of both place and gaze responses for the same target and found two peaks in the average response (Fig. 4c, blue). For each cell, we found the peak firing rate within a ±50 ms window centred around each of the two peaks. Cells were sorted on the basis of the difference in peak rate during these two windows.

Analysis of interneuron firing. We categorized the pattern of interneuron firing by first calculating the mean firing rate for each cell across

all saccades. Interneurons had some selectivity but were generally active for all saccade targets. We then performed a Hilbert transform on the mean firing rate and stored the instantaneous phase of the response at 187 ms after the saccade peak (the time of peak firing in excitatory cells; Fig. 4c). We performed circular *k*-means clustering on the instantaneous phases to classify interneurons into two groups.

Statistical analysis

All confidence intervals given in the text and figures are the mean ± s.e.m., unless otherwise specified.

Reporting summary

Further information on research design is available in the Nature Portfolio Reporting Summary linked to this article.

Data availability

Data are available at https://doi.org/10.5061/dryad.tqjq2bw9n.

Code availability

Example code is available at https://doi.org/10.5061/dryad.tqjq2bw9n.

56. Shih, S.-W., Wu, Y.-T. & Liu, J. A calibration-free gaze tracking technique. In *Proc. 15th International Conference on Pattern Recognition* 201–204 (IEEE, 2000).
57. Stahl, J. S., van Alphen, A. M. & De Zeeuw, C. I. A comparison of video and magnetic search coil recordings of mouse eye movements. *J. Neurosci. Methods* **99**, 101–110 (2000).
58. Li, D., Winfield, D. & Parkhurst, D. J. Starburst: a hybrid algorithm for video-based eye tracking combining feature-based and model-based approaches. In *Proc. 2005 IEEE Computer Society Conference on Computer Vision and Pattern Recognition (CVPR'05) Workshops* 79 (IEEE, 2005).
59. Pachitariu, M., Steinmetz, N. A., Kadir, S. N., Carandini, M. & Harris, K. D. in *Advances in Neural Information Processing Systems* Vol. 29 (Curran Associates, 2016).
60. Denovellis, E. L. et al. Hippocampal replay of experience at real-world speeds. *eLife* **10**, e64505 (2021).
61. Skaggs, W. E., McNaughton, B. L., Gothard, K. M. & Markus, E. J. in *Advances in Neural Information Processing* Vol. 5 (eds Hanson, S. J. et al.) 1030–1037 (Morgan Kaufmann, 1993)
62. Bahill, A. T., Clark, M. R. & Stark, L. The main sequence, a tool for studying human eye movements. *Math. Biosci.* **24**, 191–204 (1975).
63. Applegate, M. C., Gutnichenko, K. S., Mackevicius, E. L. & Aronov, D. An entorhinal-like region in food-caching birds. *Curr. Biol.* **33**, 2465–2477.e7 (2023).

Acknowledgements We thank S. Hale for technical assistance, Aronov laboratory members for helpful discussion, the Black Rock Forest Consortium, J. Scribner and Hickory Hill Farm, T. Green for fieldwork support, and J. Kuhl for the chickadee illustration in Fig. 1a. Funding was provided by the NIH BRAIN Initiative Advanced Postdoctoral Career Transition Award (K99 EY034700; H.L.P.), New York Stem Cell Foundation Robertson Neuroscience Investigator Award (D.A.), Beckman Young Investigator Award (D.A.), NIH New Innovator Award (DP2 AG071918; D.A.) and the Howard Hughes Medical Institute (D.A.).

Author contributions H.L.P. and D.A. designed the experiments, analysed the data and wrote the paper. H.L.P. performed the experiments.

Competing interests The authors declare no competing interests.

Additional information

Supplementary information The online version contains supplementary material available at https://doi.org/10.1038/s41586-025-09101-z.

Correspondence and requests for materials should be addressed to Hannah L. Payne or Dmitriy Aronov.

Peer review information *Nature* thanks Uwe Mayer, Jonathan Whitlock and the other, anonymous, reviewer(s) for their contribution to the peer review of this work.

Reprints and permissions information is available at http://www.nature.com/reprints.

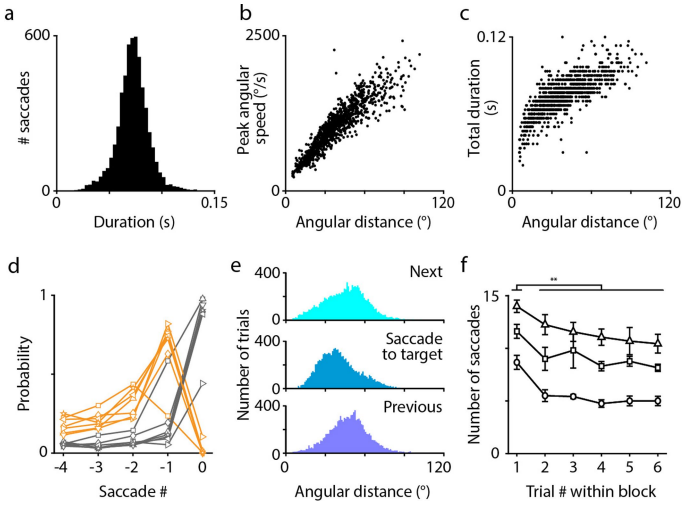

Extended Data Fig. 1 | Properties of head movements in chickadees. **(a)** Head saccade durations for an example session. **(b)** Relationship between angular distance travelled by the head and the peak angular speed during head saccades for the same session. **(c)** Relationship between distance travelled and saccade duration. Both (b) and (c) show strong correlations, illustrating similarities to the eye saccade main sequence in primates[62]. **(d)** Time courses of the two gaze strategies (*orange*: lateral; *black*: frontal). Each line represents one bird. Data are shown as in Fig. 1g, but for all 7 birds recorded in the X-shaped arena, averaged across sessions. **(e)** Distribution of saccade angular distances for saccades that successfully land on an unrewarded target site, as well as for the preceding and following saccades. Gazes that land on the target are produced by smaller saccades (median saccade distance 38.7° for the saccade to the target, 47.8° preceding saccade, 46.0° next saccade; saccade to target vs. previous and next, $p = 0.0004$ and 0.0009, two sided t-tests conducted on the median distances for each bird, $n = 7$ birds recorded in the X-shaped arena). This implies that gaze locations that precede successful target hits are, on average, slightly closer to the target than other gaze locations. **(f)** Number of saccades required by birds in the Blocked trial task to find the correct target. Each line represents one bird, error bars indicate mean ± S.E.M. across the medians for each session ($n = 8, 13, 6$ sessions for the three birds from top to bottom). Chickadees take longer to find the target on the first trial (when they have no information about which target is rewarded) than on subsequent trials ($p = 0.007, 0.006, 4 \times 10\text{-}8$, two-sided t-test conducted separately for each bird). Note that when shifting gaze from one target to another, birds often make several intermediate saccades at other points in the environment.

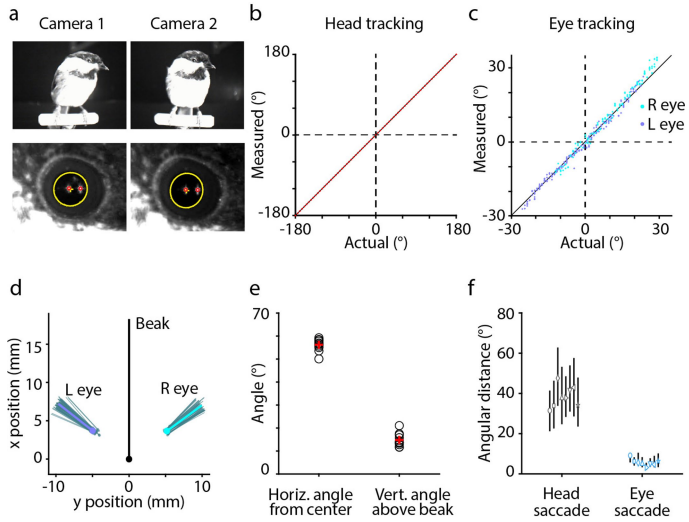

Extended Data Fig. 2 | Eye tracking method and properties of eye movements in chickadees. (a) Video-oculography using two infrared light sources. The chickadee is perched close to two cameras, which acquire video frames from slightly different angles (*top*). The pupil (yellow) and the corneal reflections of the two light sources (*red*) are detected in the videos. Head tracking is conducted simultaneously using an array of infrared reflective markers attached to the bird's implant (*not shown*). **(b)** Accuracy of head tracking: 0.046° root-mean-squared error (RMSE). *Red dots*: measurement; *Black line*: unity line. **(c)** Accuracy of eye tracking: 1.78° RMSE measured across fixations, 1.79° measured across individual frames. *Dots*: individual fixations. **(d)** Position of the eye (*dots*) and the orientation of the optical axis (*lines*) relative to the head. Projections onto the horizontal axis are shown. *Gray*: individual video frames for a single calibration experiment. *Blue*: average across frames. **(e)** Orientation of the optical axis across all birds (*black symbols*) and the average across birds (*red symbols*). **(f)** Angular displacement of the head and the eye during head saccades. Symbols indicate medians for each bird; lines indicate 25th and 75th percentiles (n = 4341 – 144521 head saccades per bird, n = 8 – 55 eye saccades per bird).

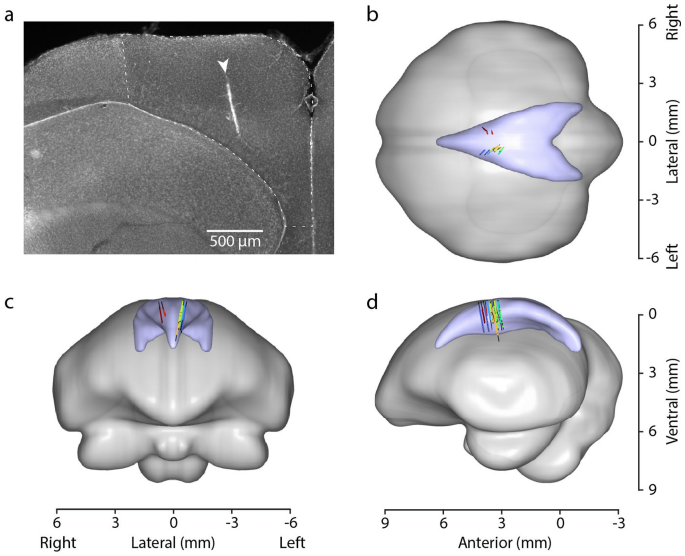

Extended Data Fig. 3 | Histological analysis of recording locations. **(a)** Coronal section of a typical recording location in the hippocampus, showing the track of the recording probe. The section is labeled with DAPI, which clearly delineates the lower-density hippocampus from the higher-density dorsolateral region (DL) that is directly lateral to the hippocampus. **(b-d)** Locations of all recorded cells registered to a 3D model of the chickadee brain constructed using data from[63]. *Colored symbols:* cells included in the paper, *black lines:* electrode tracks. Track locations were confirmed histologically for 8/14 probe tracks, yielding 2504/2658 cells in the X-shaped tasks and 351/361 cells in the all-to-all task (note that 5/9 birds were implanted with two-shank silicon probes). The locations of the remaining cells were estimated from stereotaxic coordinates. Lambda is located at 0 mm in the displayed coordinate axes.

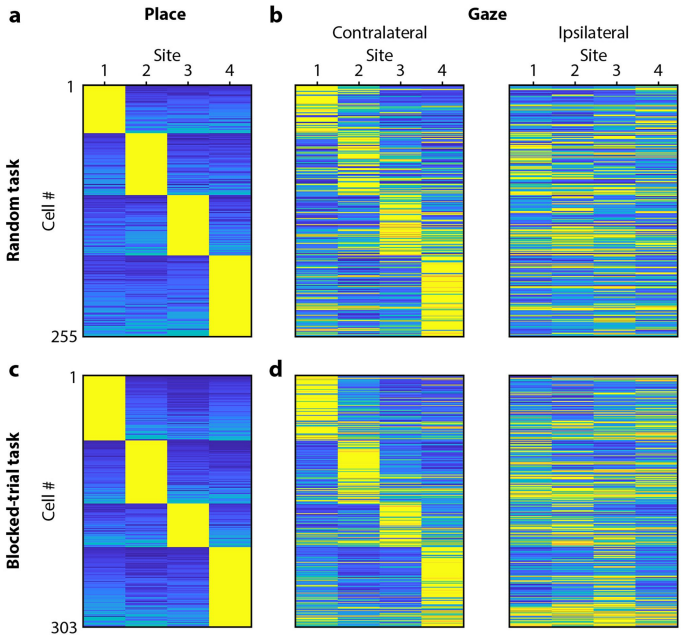

Extended Data Fig. 4 | Comparison of place and gaze coding across tasks. **(a-b)** Place and gaze coding, shown as in Fig. 2e,f, but only for cells recorded in the Random task, where the location of the rewarded target was chosen randomly on each trial. Each row is separately normalized from 0 (blue) to the maximum (yellow). **(c-d)** Same, but only for cells recorded in the Blocked-trial task, where the same rewarded target was repeated for six trials in a row.

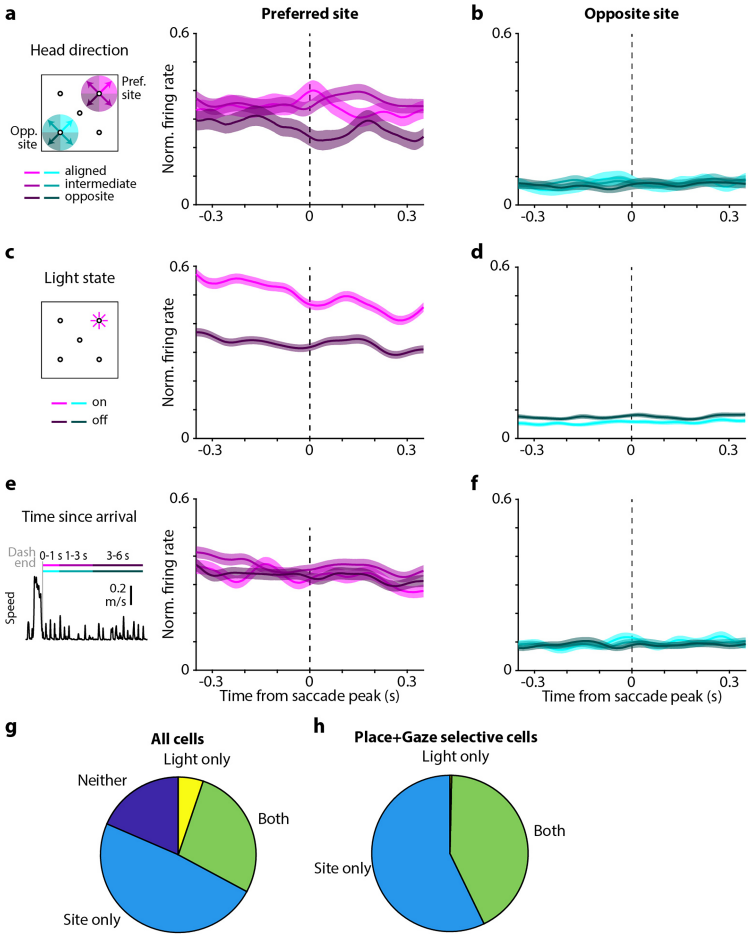

Extended Data Fig. 5 | Place coding is not explained by simple visual responses. (a-b) Saccade-aligned firing rates averaged across cells, when the bird is located at one of the corner target sites, but gazing elsewhere in the environment. Included are cells with place and gaze selectivity (>0.5) for one of the sites. For each cell, firing rates are plotted for trials when the bird is at that cell's preferred site and when the bird is at the opposite site. Saccades are grouped according to the azimuthal direction the bird is facing. To eliminate saccades in which the bird is gazing down at the feeder, saccades are only included if the elevation of gaze is within ±30° elevation from the average vector of gaze at targets within each session (average elevation −9° across sessions). The direction of gaze is given by the contralateral eye. In all cases, cells remain selective for the bird's location at their preferred site. Error bars indicate mean ± S.E.M. across cells. **(c-d)** Same as (a-b), but saccades are grouped according to whether the indicator light is on or already turned off. Although cells respond more strongly when the light is on at their preferred site, this response does not explain their site preference. **(e-f)** Same as (a-b), but saccades are grouped according to the time after the bird's arrival at the target site. Elapsed time does not explain the site preference. **(g)** Results of a generalized linear model that evaluated each cell's tuning for gaze location and the state of the viewed light cue (on or off). For each saccade, we counted spikes from −100 to +300 ms, and for each cell used the MATLAB function fitglme with a log link function and Poisson distribution. Very few cells (5.2%, 131/2524 with a statistical threshold of p = 0.05, two-sided log-likelihood ratio test) were tuned to the indicator light without also being location-tuned. **(h)** Same as (g), but for the 278 cells that had place and gaze selectivity of >0.5. Only one cell was significantly light-tuned without also being location-tuned.

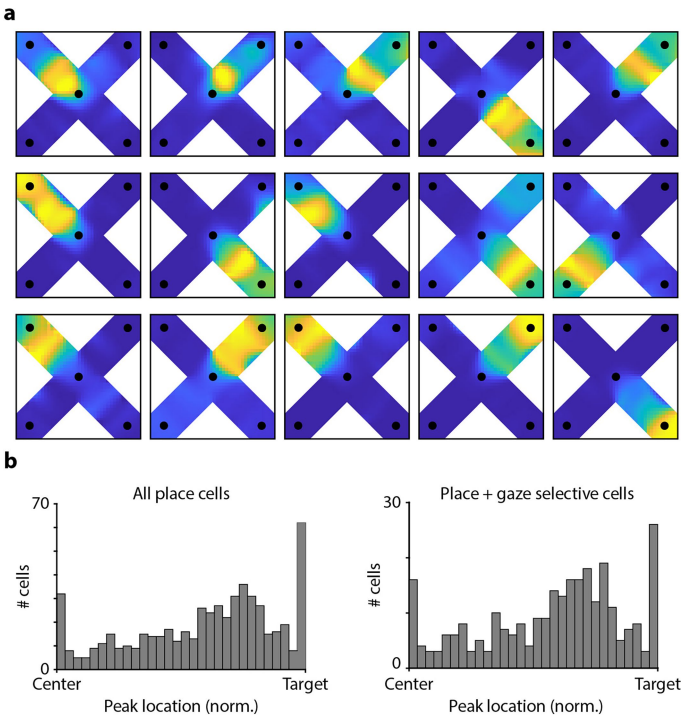

Extended Data Fig. 6 | Distribution of place fields in the arena. (a) Example place maps for neurons that had firing fields at various locations along the path of the bird. In order to match the conventional way place cells are analyzed in the literature, spikes are not shifted by the optimal time lag for each neuron. Otherwise, the maps are plotted as in Fig. 1c. **(b)** Distribution of place field locations for all place cells (*left*) and only cells with place and gaze selectivity >0.5 (*right*). Place field location was defined as the location of the maximum firing rate for each cell. The first and last bin of the histogram are over-represented because the maximum was measured on a truncated segment of the arena between the central site and the target. Although more cells have place fields closer to the target than to the center, there are many cells with place fields far from the target that have significant gaze coding (*right*).

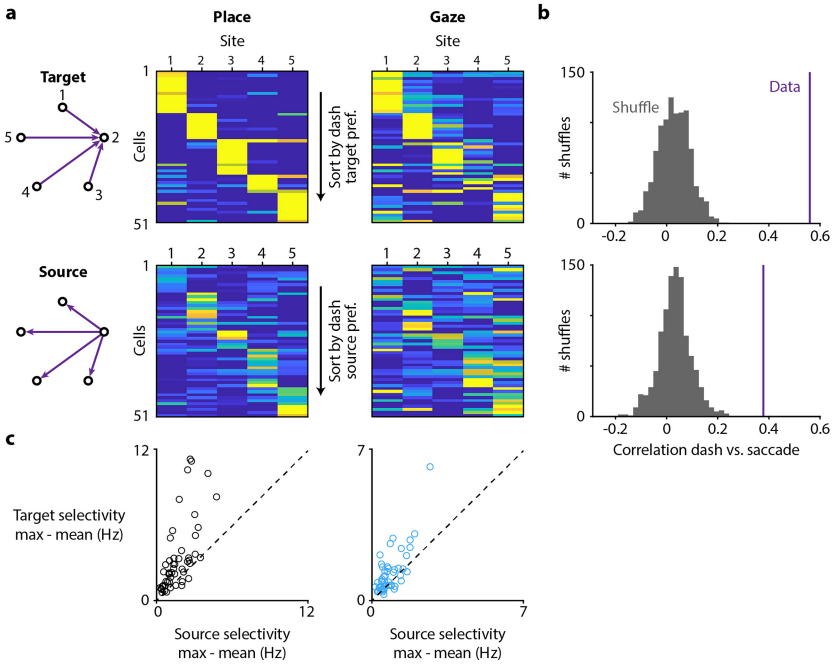

Extended Data Fig. 7 | All-to-all task to disambiguate gaze target from the bird's location. (a) Activity in the All-to-all task, where the chickadee was located at one of five sites and gazing at one of the other sites. After this visual search period, the chickadee dashed directly from one site to another. The location of the bird prior to the dash was the "source", while the target of gaze and the endpoint of the dash was the "target". Activity of each cell is shown during dashes ("Place", *left*) and during gaze fixations ("Gaze", *right*). Firing rates are calculated as a function of either the target site (*top*) or the source site (*bottom*). Included are cells with place and gaze selectivity (>0.67), either for the target or the source, and with baseline-subtracted response > 0.5 Hz. Each row is normalized from 0 (*blue*) to maximum (*yellow*) across target and source measurements, separately for place and gaze. **(b)** Correlation of the tuning curves for place and gaze (i.e. the rows of the matrices in (a)). *Top*: correlation of target tuning curves; *bottom*: correlation of source tuning curves. In both cases, correlations for actual data are higher than for a shuffled distribution, in which cell identities were scrambled. **(c)** Comparison of selectivity for target and for source. Selectivity for each neuron was measured by subtracting the mean of the five values in its tuning curve from the maximum of those five values. For both place (*left*) and gaze (*right*), selectivity is higher for the target than for the source.

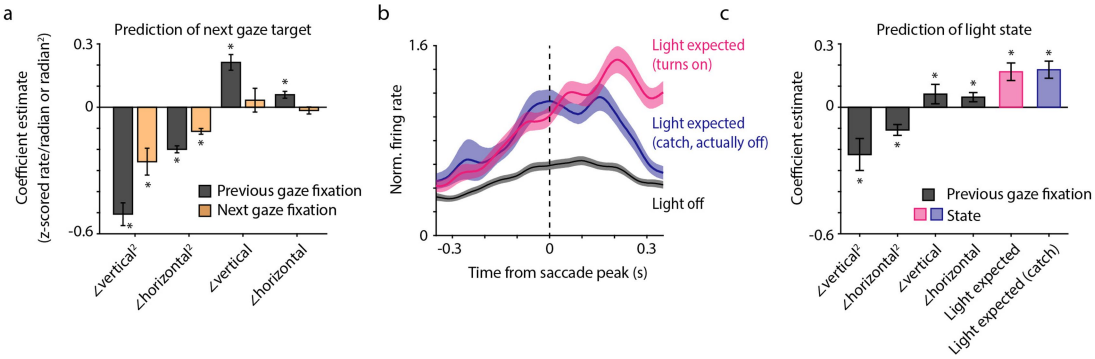

Extended Data Fig. 8 | Early peak during gaze fixations partly predicts the upcoming gaze. (a) Coefficients of a linear mixed effects model that fit the early response (at +17 ms relative to saccade peak) as a function of eight behavioral variables (fixed effects), and allowed the intercept to vary for each cell (random effect). Four of the variables accounted for the gaze fixation preceding the saccade, and the other four accounted for the gaze fixation following the saccade. For the previous and next fixation, variables included the horizontal and vertical deviations from the target (which could be positive or negative), as well as the squared values of these deviations. Included are cells with place and gaze selectivity >0.5 (n = 278 cells). Asterisks indicate significant coefficients ($p < 10^{-9}$ for all, p-value for the t-statistic of the hypothesis that the corresponding coefficient is different from zero, returned by MATLAB function fitlme. We then adjusted each p-value for multiple comparisons using a Bonferroni correction). Error bars indicate 95% confidence intervals for the coefficient estimates. The key conclusion is that the early response depended on the location of the next fixation. **(b)** Same as Fig. 3h, but only including trials where the previous fixation was 30–40° from the preferred target. Note that the early response still depends on the bird's expectation of the light turning on, even though the previous fixation is clamped in the same narrow range of angles for all conditions. Due to the small subset of trials, the number of included cells is now smaller than in Fig. 3h (n = 387, 377, and 364 cells for the *black*, *blue*, and *pink* traces). **(c)** Coefficients of a model that fit the early response in the Blocked-trial task and included variables for whether the chickadee should expect the light to turn on in the trial, separately for catch and non-catch trials. In both cases, coefficients corresponding to these variables were significantly non-zero (* indicates $p < 0.05$, calculated as in panel (a)), indicating that the early response predicted whether the light would turn on. For (c), included cells were the same as in Fig. 3h (n = 402 cells).

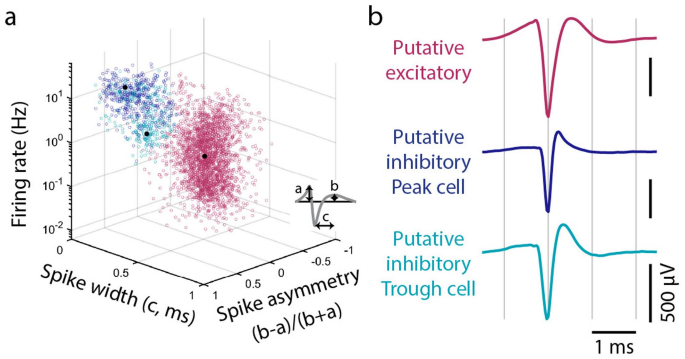

Extended Data Fig. 9 | Classification of cell types in the chickadee hippocampus. (a) All recorded units plotted according to their mean firing rate across the session and two features of spike waveforms shown in the diagram. These measurements separate putative excitatory (*pink*) from putative inhibitory (*blue* and *teal*) cells. Inhibitory cells are further classified by their responses during saccades (Fig. 4) into Peak (*blue*) and Trough (*teal*) types; these types show some systematic differences in firing rate and spike waveforms. **(b)** Average spike waveforms of three example cells, one from each of the categories shown in (a).

nature portfolio

Corresponding author(s): Dmitriy Aronov, Hannah Payne

Last updated by author(s): Apr 29, 2025

Reporting Summary

Nature Portfolio wishes to improve the reproducibility of the work that we publish. This form provides structure for consistency and transparency in reporting. For further information on Nature Portfolio policies, see our Editorial Policies and the Editorial Policy Checklist.

Statistics

For all statistical analyses, confirm that the following items are present in the figure legend, table legend, main text, or Methods section.

n/a	Confirmed	
☐	☒	The exact sample size (*n*) for each experimental group/condition, given as a discrete number and unit of measurement
☐	☒	A statement on whether measurements were taken from distinct samples or whether the same sample was measured repeatedly
☐	☒	The statistical test(s) used AND whether they are one- or two-sided *Only common tests should be described solely by name; describe more complex techniques in the Methods section.*
☐	☒	A description of all covariates tested
☒	☐	A description of any assumptions or corrections, such as tests of normality and adjustment for multiple comparisons
☐	☒	A full description of the statistical parameters including central tendency (e.g. means) or other basic estimates (e.g. regression coefficient) AND variation (e.g. standard deviation) or associated estimates of uncertainty (e.g. confidence intervals)
☐	☒	For null hypothesis testing, the test statistic (e.g. *F*, *t*, *r*) with confidence intervals, effect sizes, degrees of freedom and *P* value noted *Give P values as exact values whenever suitable.*
☒	☐	For Bayesian analysis, information on the choice of priors and Markov chain Monte Carlo settings
☒	☐	For hierarchical and complex designs, identification of the appropriate level for tests and full reporting of outcomes
☐	☒	Estimates of effect sizes (e.g. Cohen's *d*, Pearson's *r*), indicating how they were calculated

Our web collection on statistics for biologists contains articles on many of the points above.

Software and code

Policy information about availability of computer code

Data collection	Intan USB Interface Board software and Qualisys Track Manager were used to collect electrophysiological and behavioral data, respectively. MATLAB code was used to control and record the experimental state.
Data analysis	Spike sorting was performed using Kilosort 2.0 (MATLAB, archive available at https://github.com/hpay/spikesort-hp-2025), annotated in Phy (Python), and analyzed in MATLAB. Eye tracking code is available at https://github.com/hpay/eyetrack-bird. Sample analysis code is available at https://doi.org/10.5061/dryad.tqjq2bw9n

For manuscripts utilizing custom algorithms or software that are central to the research but not yet described in published literature, software must be made available to editors and reviewers. We strongly encourage code deposition in a community repository (e.g. GitHub). See the Nature Portfolio guidelines for submitting code & software for further information.

Data

Policy information about availability of data

All manuscripts must include a data availability statement. This statement should provide the following information, where applicable:

- Accession codes, unique identifiers, or web links for publicly available datasets
- A description of any restrictions on data availability
- For clinical datasets or third party data, please ensure that the statement adheres to our policy

Data are available at https://doi.org/10.5061/dryad.tqjq2bw9n

Research involving human participants, their data, or biological material

Policy information about studies with human participants or human data. See also policy information about sex, gender (identity/presentation), and sexual orientation and race, ethnicity and racism.

Reporting on sex and gender	n/a
Reporting on race, ethnicity, or other socially relevant groupings	n/a
Population characteristics	n/a
Recruitment	n/a
Ethics oversight	n/a

Note that full information on the approval of the study protocol must also be provided in the manuscript.

Field-specific reporting

Please select the one below that is the best fit for your research. If you are not sure, read the appropriate sections before making your selection.

☒ Life sciences ☐ Behavioural & social sciences ☐ Ecological, evolutionary & environmental sciences

For a reference copy of the document with all sections, see nature.com/documents/nr-reporting-summary-flat.pdf

Life sciences study design

All studies must disclose on these points even when the disclosure is negative.

Sample size	Sample size calculation was not performed prior to the start of the study. The number of birds is consistent with sample sizes in related studies (Payne, Lynch, Aronov 2021; Chettih et al. 2024). The number of cells recorded per bird varied due to experimental chance
Data exclusions	Cells were excluded if they were deemed to be outside of the hippocampus, as described in Methods. Recording sessions were not included if insufficient trials (dashes or saccades) were performed.
Replication	We replicated each finding across multiple birds: 7 birds in the Random task, 3 in the Blocked-trial task, and 3 in the All-to-all task.
Randomization	Not applicable, no experimental/treatment groups.
Blinding	Experiments were conducted blind to sex.

Reporting for specific materials, systems and methods

We require information from authors about some types of materials, experimental systems and methods used in many studies. Here, indicate whether each material, system or method listed is relevant to your study. If you are not sure if a list item applies to your research, read the appropriate section before selecting a response.

Materials & experimental systems

n/a	Involved in the study
☒	☐ Antibodies
☒	☐ Eukaryotic cell lines
☒	☐ Palaeontology and archaeology
☐	☒ Animals and other organisms
☒	☐ Clinical data
☒	☐ Dual use research of concern
☒	☐ Plants

Methods

n/a	Involved in the study
☒	☐ ChIP-seq
☒	☐ Flow cytometry
☒	☐ MRI-based neuroimaging

Animals and other research organisms

Policy information about studies involving animals; ARRIVE guidelines recommended for reporting animal research, and Sex and Gender in Research

Laboratory animals	The study did not involve laboratory animals
Wild animals	Male and female Black-capped chickadees (poecile atricapillus) were collected from the Black Rock Forest Consortium, Hickory Hill Farm, Taconic State Park, and Brookhaven National Laboratory. Animals were collected and transported according to federal and state scientific collection permits and a Columbia University IACUC-approved protocol. Collection occurred primarily in fall and early winter using the mist netting technique. Exact age is unknown, but based on the date of capture relative to seasonal breeding patterns all birds were at least 6 months of age. Animals were euthanized after recordings were complete as described in Methods, in order to determine neural recording locations.
Reporting on sex	Experiments were conducted blind to sex and sample sizes are reported. Foraging behavior is not known to differ between male and female chickadees.
Field-collected samples	The study did not involve field samples.
Ethics oversight	All animal procedures were approved by the Columbia University Institutional Animal Care and Use Committee and carried out in accordance with the US National Institutes of Health guidelines.

Note that full information on the approval of the study protocol must also be provided in the manuscript.

Plants

Seed stocks	*Report on the source of all seed stocks or other plant material used. If applicable, state the seed stock centre and catalogue number. If plant specimens were collected from the field, describe the collection location, date and sampling procedures.*
Novel plant genotypes	*Describe the methods by which all novel plant genotypes were produced. This includes those generated by transgenic approaches, gene editing, chemical/radiation-based mutagenesis and hybridization. For transgenic lines, describe the transformation method, the number of independent lines analyzed and the generation upon which experiments were performed. For gene-edited lines, describe the editor used, the endogenous sequence targeted for editing, the targeting guide RNA sequence (if applicable) and how the editor was applied.*
Authentication	*Describe any authentication procedures for each seed stock used or novel genotype generated. Describe any experiments used to assess the effect of a mutation and, where applicable, how potential secondary effects (e.g. second site T-DNA insertions, mosiacism, off-target gene editing) were examined.*